Award Number: W81XWH-09-1-0726

TITLE: "CINRG: Systems Biology of Glucocorticoids in Muscle Disease."

PRINCIPAL INVESTIGATOR: Zuyi Wang, PhD

CONTRACTING ORGANIZATION: Children's Research Institute
Washington DC, 20010

REPORT DATE: December 2014

TYPE OF REPORT: Addendum to Final report

PREPARED FOR: U.S. Army Medical Research and Materiel Command
Fort Detrick, Maryland 21702-5012

DISTRIBUTION STATEMENT:

X Approved for public release; distribution unlimited

REPORT DOCUMENTATION PAGE

Form Approved
OMB No. 0704-0188

1. REPORT DATE *(DD-MM-YYYY)*	2. REPORT TYPE	3. DATES COVERED *(From - To)*
December 2014	Addendum to Final report	21Sep2013 - 20Sep2014

4. TITLE AND SUBTITLE

"CINRG: Systems Biology of Glucocorticoids in Muscle Disease."

5a. CONTRACT NUMBER
W81XWH-09-1-0726

5b. GRANT NUMBER

5c. PROGRAM ELEMENT NUMBER

6. AUTHOR(S)
Zuyi Wang, PhD

email: zwang@cnmcresearch.org

5d. PROJECT NUMBER

5e. TASK NUMBER

5f. WORK UNIT NUMBER

7. PERFORMING ORGANIZATION NAME(S) AND ADDRESS(ES)

Children's Research Institute
111 Michigan Ave NW
Washington DC, 20010

8. PERFORMING ORGANIZATION REPORT NUMBER

9. SPONSORING / MONITORING AGENCY NAME(S) AND ADDRESS(ES)

U.S. Army Medical Research and Materiel Command
Fort Detrick, Maryland 21702-5012

10. SPONSOR/MONITOR'S ACRONYM(S)

11. SPONSOR/MONITOR'S REPORT NUMBER(S)

12. DISTRIBUTION / AVAILABILITY STATEMENT

Approved for public release; distribution unlimited

13. SUPPLEMENTARY NOTES

14. ABSTRACT

This is the addendum of the final report, and we report here the accomplishments and progress made during the extension period, September 21, 2013 to September 20, 2014. We published a paper on Journal of Cell Biology to report our experimental and data analysis results on asynchronous remodeling in dystrophic muscles in Duchenne muscular dystrophy. One doctoral student who were under partial support from this grant graduated in the summer of 2014.

15. SUBJECT TERMS

Duchenne Muscular dystrophy, Glucocorticoids, Systems biology, Drug mechanism

16. SECURITY CLASSIFICATION OF:			17. LIMITATION OF ABSTRACT	18. NUMBER OF PAGES	19a. NAME OF RESPONSIBLE PERSON
a. REPORT	b. ABSTRACT	c. THIS PAGE			19b. TELEPHONE NUMBER *(include area code)*
U	U	U	UU	30	USAMRMC

Standard Form 298 (Rev. 8-98)
Prescribed by ANSI Std. Z39.18

Table of Contents

Addendum of Final progress report for Contract W81XWH-09-1-0726

SYSTEMS BIOLOGY OF GLUCOCORTICOIDS IN MUSCLE DISEASE

Reportable Outcomes (during September 21, 2013 to September 20, 2014)

1. The work, partially supported by this grant, on asynchronous remodeling in dystrophic muscles in Duchenne muscular dystrophy has been published (see attachment):
   Dadgar S, Wang Z, Johnston H, Kesari A, Nagaraju K, Chen YW, Hill DA, Partridge TA, Giri M, Freishtat RJ, Nazarian J, Xuan J, Wang Y, Hoffman EP. "Asynchronous remodeling is a driver of failed regeneration in Duchenne muscular dystrophy." *J Cell Biol*. 2014 Oct 13;207(1):139-58. doi: 10.1083/jcb.201402079. (Dadgar S, Wang Z, Johnston H contributed equally to this paper.)
2. Partially supported and closely related to the research of this grant, the PI, Dr. Zuyi Wang, led a study on natural history of childhood asthma symptoms and the influence of sex and age (see attachment):
   Fu L, Freishtat RJ, Gordish-Dressman H, Teach SJ, Resca L, Hoffman EP, Wang Z. "Natural progression of childhood asthma symptoms and strong influence of sex and puberty." *Ann Am Thorac Soc.* 2014 Jul;11(6):939-44. doi: 10.1513/AnnalsATS.201402-084OC.
3. Dr. Helen Carey-Johnston, who was partially supported by this grant, has recently defended her doctoral dissertation in the summer of 2014, and obtained her PhD degree in Biology from George Washington University. Her advisor is Dr. Eric Hoffman. Her dissertation topic focused on developing the asynchronous regeneration model in normal muscles to simulate the asynchronous remodeling in dystrophic muscles, and the effect of glucocorticoid drugs in reducing the asynchrony. Her work has been reported in the progress reports and the publication on Journal of Cell Biology (listed above).

Published October 13, 2014

Asynchronous remodeling is a driver of failed regeneration in Duchenne muscular dystrophy

Sherry Dadgar,[1,2] Zuyi Wang,[1,2] Helen Johnston,[1,2] Akanchha Kesari,[1,2] Kanneboyina Nagaraju,[1,2] Yi-Wen Chen,[1,2] D. Ashley Hill,[1,2] Terence A. Partridge,[1,2] Mamta Giri,[1,2] Robert J. Freishtat,[1,2] Javad Nazarian,[1,2] Jianhua Xuan,[3] Yue Wang,[3] and Eric P. Hoffman[1,2]

[1]Center for Genetic Medicine Research, Children's National Medical Center, and [2]Department of Integrative Systems Biology, George Washington University, Washington, DC 20010
[3]The Bradley Department of Electrical and Computer Engineering, Virginia Polytechnic Institute and State University, Arlington, VA 24061

We sought to determine the mechanisms underlying failure of muscle regeneration that is observed in dystrophic muscle through hypothesis generation using muscle profiling data (human dystrophy and murine regeneration). We found that transforming growth factor β–centered networks strongly associated with pathological fibrosis and failed regeneration were also induced during normal regeneration but at distinct time points. We hypothesized that asynchronously regenerating microenvironments are an underlying driver of fibrosis and failed regeneration. We validated this hypothesis using an experimental model of focal asynchronous bouts of muscle regeneration in wild-type (WT) mice. A chronic inflammatory state and reduced mitochondrial oxidative capacity are observed in bouts separated by 4 d, whereas a chronic profibrotic state was seen in bouts separated by 10 d. Treatment of asynchronously remodeling WT muscle with either prednisone or VBP15 mitigated the molecular phenotype. Our asynchronous regeneration model for pathological fibrosis and muscle wasting in the muscular dystrophies is likely generalizable to tissue failure in chronic inflammatory states in other regenerative tissues.

Introduction

Duchenne muscular dystrophy (DMD) is a relatively common inborn error, caused by lack of dystrophin in the membrane cytoskeleton of muscle fibers (Hoffman et al., 1987). Myofibers show increased plasma membrane instability and can undergo cell death (necrosis) either individually or in groups. Necrotic myofibers are able to regenerate within the preexisting basal lamina through satellite cell activation, myoblast proliferation, fusion, and maturation—a process that takes ∼2 wk. Robust regeneration is seen in young DMD patient muscle as well as dystrophin-deficient dogs, mice, cats, and pigs (Chen et al., 2005; Kornegay et al., 2012a; Klymiuk et al., 2013). Successful regeneration is associated with retained muscle function at a young age. However, as a DMD patient ages, muscle regeneration gradually fails, with endomysial fibrosis and fatty replacement of the muscle. The fibrofatty infiltration is typically commensurate with muscle wasting and loss of muscle function. Some muscles in both dystrophin-deficient DMD patients and dogs, such as the extraocular muscles and sartorius, seem able to maintain regeneration and are functionally spared (Kornegay et al., 2012b; Nghiem et al., 2013). Most dystrophin-deficient muscles in cats and mice are able to successfully regenerate throughout the normal life span (Gaschen et al., 1992). The failed regeneration seen in the DMD muscle has features that are shared with aging muscle, including chronic inflammatory state and loss of mitochondrial function (Baron et al., 2011). However, the age-, muscle-, and species-specific progressions from successful to failed regeneration are poorly understood, and there has not been a unifying model able to explain the observed transition to muscle wasting and the loss of muscle function (Serrano et al., 2011).

S. Dadgar, Z. Wang, and H. Johnston contributed equally to this paper.

Correspondence to Eric P. Hoffman: ehoffman@childrensnational.org

Abbreviations used in this paper: ALS, amyotrophic lateral sclerosis; BMD, Becker muscular dystrophy; COX, cytochrome *c* oxidase; DMD, Duchenne muscular dystrophy; FSH, facioscapulohumeral dystrophy; JDM, juvenile dermatomyositis; LCM, laser capture microscopy; NHM, normal human skeletal muscle; qRT-PCR, quantitative RT-PCR; SDH, succinate dehydrogenase; WT, wild type.

Supplemental Material can be found at:
http://jcb.rupress.org/content/suppl/2014/10/09/jcb.201402079.DC1.html
http://jcb.rupress.org/content/suppl/2014/10/13/jcb.201402079.DC2.html

The Rockefeller University Press $30.00
J. Cell Biol. Vol. 207 No. 1 139–158
www.jcb.org/cgi/doi/10.1083/jcb.201402079

Published October 13, 2014

The gradual loss of muscle tissue and disorganization of muscle structure in most muscles in a DMD patient has been attributed, in part, to a progressive exhaustion of satellite cell function in response to the chronic drive to repair degenerating muscle fibers (Blau et al., 1983). However, there are conflicting studies regarding the number and nature of muscle stem cells, and loss of satellite cells with age is questioned as there appear to be higher numbers of satellite cells in DMD muscle than there are in normal muscle (Watkins and Cullen, 1986, 1988; Maier and Bornemann, 1999; Kottlors and Kirschner, 2010). Reports of diminished DMD myoblast proliferation have been associated with low minimal telomere length in DMD whole muscle (Aguennouz et al., 2011) and myoblasts (Decary et al., 2000). However, this remains controversial as another investigation detected no overall reduction in mean telomere length in DMD muscle cells (Oexle et al., 1997).

An alternative hypothesis promoted for failed regeneration is the excessive connective tissue proliferation (fibrosis), a feature in common with many chronic inflammatory states (Serrano et al., 2011). Fibrosis could impair vascularization of muscle tissue, create an insufficient environment for effective satellite cell proliferation and differentiation, and alter cell–cell communication during myofiber regeneration. Histologically, fibrosis is characterized by the exaggerated expression and deposition of extracellular matrix components, particularly collagen I. TGF-β, a key cytokine promoting fibrosis, appears to have a critical role in fibrosis in DMD (Chen et al., 2005; MacDonald and Cohn, 2012) as well as most fibrotic states in most tissues (Akhurst and Hata, 2012; Bowen et al., 2013). Strong induction of TGF-β pathways is seen in both successful and unsuccessful remodeling (Karkampouna et al., 2012). Indeed, TGF-β is important for normal muscle regeneration, and the molecular mechanisms underlying a change in normal versus pathological roles of TGF-β pathways have remained elusive for muscular dystrophy and other chronic inflammatory states (Bhattacharyya et al., 2013). The likely importance of TGF-β pathways in DMD is underscored by the recent finding of two genetic modifiers of disease severity, both of which map to TGF-β pathways (SPP1/osteopontin [Pegoraro et al., 2011; Bello et al., 2012]; LTPB4 [Flanigan et al., 2013]).

Here, we used a data-driven approach involving three large mRNA profiling experiments (two human muscle biopsy and one murine regeneration series) to generate a novel hypothesis regarding the cellular underpinnings of failed regeneration in muscle disease (asynchronous regeneration). The hypothetical model was then tested using an experimental approach of asynchronous bouts of staged degeneration/regeneration in localized microenvironments of wild-type (WT) muscle.

Results

Development of bioinformatics methods for increased sensitivity of biochemical network selection

It is well documented that different analytical methods applied to the same microarray dataset can provide very different interpretations of the data, often with only 30% concordance of lists of differentially regulated genes (Bakay et al., 2002; Seo et al., 2004, 2006; Irizarry et al., 2005). We reasoned that increased sensitivity for selection of differentially regulated genes could be obtained by using multiple probe set algorithms, multiple microarrays (e.g., U133A and U133B arrays on the same samples), and multiple queries of existing literature for biochemical pathways (Fig. S1). Such an iterative approach would be expected to greatly increase sensitivity of gene selection but also increase false positives. However, using an integrative approach with a composite score of gene selection and associated networks, we could decrease false positives by focusing on the top-ranked composite networks (Fig. S1). In effect, as different sources of data are assembled to derive a probability determining the specificity of a network, the most highly scored networks have considerable statistical power and significance.

To our knowledge, this two-tier composite approach has not been previously described. This approach would be expected to be most effective on larger and more complex datasets, and for this reason, we used a human 12-disease group, 117-biopsy dataset, and 234-microarray dataset as a dataset for model generation, with multiple validation and model extension datasets.

Visualization of domain knowledge identifies a potential disease grouping by the histological phenotype of fibrosis and failed regeneration

Seven heat maps with clear patterns of association of disease groups were generated and visually inspected for possible shared pathogenesis between the clustered disease groups. Many of the disease groupings were expected and were not studied further. For example, juvenile dermatomyositis (JDM) is classified as an autoimmune disorder and shows extensive inflammation (immune cells) infiltrating the muscle (Tezak et al., 2002; Chen et al., 2008). Indeed, a strong clustering of JDM distinct from all other disorders was seen with both A and B chips and all probe set algorithms, and the members of this cluster were transcripts involved in immune cell infiltration (unpublished data). Likewise, most muscular dystrophies show some degeneration and regeneration of myofibers, and these gene clusters were evident as a recapitulation of embryonic developmental programs (unpublished data).

One particular grouping of the seven primary heat maps was believed to be particularly interesting based upon domain knowledge and was studied in some depth (Fig. 1 A). This grouping showed a strong up-regulation of transcripts in three disorders: DMD, JDM, and ED-D (Emery–Dreifuss muscular dystrophy autosomal dominant; LMNA [lamin A/C] mutations). The same cluster was up-regulated, but to a lesser extent, in Becker muscular dystrophy (BMD; dystrophin mutation), LGMD2A (limb girdle muscular dystrophy type 2A; CALP3 [calpain 3] mutation), and LGMD2B (limb girdle muscular dystrophy type 2B; DYSF [dysferlin] mutation). The clustering was seen for the A microarray and PLIER (Probe Logarithmic Intensity Error) probe set algorithm (Fig. 1, heat map) and also all other applied probe set algorithms (not depicted). This grouping could be potentially significant, as these three disorders often

Published October 13, 2014

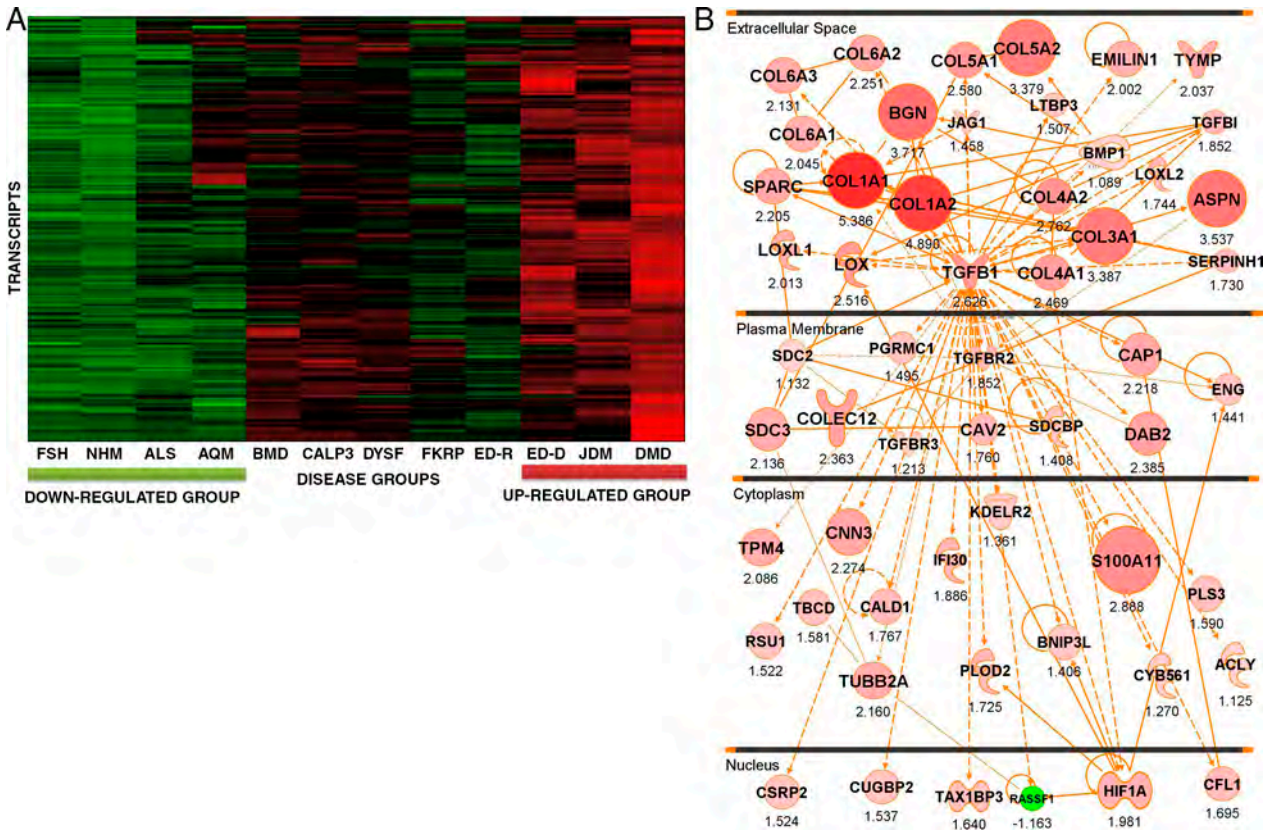

Figure 1. **An iterative composite scoring bioinformatics approach identifies a transcript network associated with progressive muscular dystrophy.** (A) Shown is a heat map of 117 muscle biopsies grouped by diagnostic category. The individual transcripts (y axis) defining this disease clustering were used to generate the molecular network in B. Disorders studied were facioscapulohumeral muscular dystrophy (FSH), normal human skeletal muscle (NHM), amyotrophic lateral sclerosis (ALS), acute quadriplegic myopathy (AQM), Becker muscular dystrophy (BMD), LGMD2A (CALP3), LGMD2B (DYSF), LGMD2I (FKRP), Emery–Dreifuss muscular dystrophy X-linked (EMRN [emerin]), Emery–Dreifuss muscular dystrophy autosomal dominant (ED-D; LMNA mutations), juvenile dermatomyositis (JDM), and Duchenne muscular dystrophy (DMD). (B) Shown is the integration of component mRNAs from the clustering in A into functional relationships based upon the literature (IPA). The top-ranked Ingenuity networks were merged into a 56-transcript network. This network is seen to be centered on TGF-β and fibrosis (collagens and other extracellular matrix transcripts), and the network is visualized based on the typical subcellular localization of the encoded proteins of each transcript. Red symbols represent up-regulated transcripts, with the size of the symbol and intensity of color scaled to the observed fold change between groups (DMD, JDM, and ED-D vs. FSH, ALS, and NHM), with fold change with the PLIER algorithm provided under each symbol. Statistical data corresponding to this network are provided in Table 1.

show particularly severe histological patterns of fibrosis and failed regeneration early in the disease process.

As shown in Fig. S1, this grouping was expanded to both A and B microarrays and both PLIER and dCHIP (DNA chip analyzer) probe set algorithms. Applying IPA (Ingenuity Pathway Analysis) to this clustering, we found the top-ranked networks to share many component members, and these were merged into a 56-member network (Fig. 1 B). Fold changes were displayed using both node size and intensity of color, with the numeric value shown under each node. Statistical support for differential regulation of component members is shown for the PLIER algorithm (Table 1).

This network was centered on TGF-β, a well-studied cytokine associated with pathological fibrosis in many tissues (Akhurst and Hata, 2012; Bowen et al., 2013) and included many of the known components of fibrotic tissue (collagens and lysine oxygenases). Another notable component of the network was HIF1A (hypoxia-inducible factor 1, α subunit), a known transcription factor strongly induced by tissue ischemia (Koh and Powis, 2012). The nature of the network suggested that it was simply reflective of a more severe pathology (greater fibrosis, greater failed remodeling, and regeneration), and DMD, JDM, and LMNA often (but not always) show more severe pathology at the initial diagnosis compared with the other disorders in the dataset.

To test whether the network was more reflective of tissue pathology than clinical and molecular diagnosis, a second validation dataset was generated that was then analyzed by unsupervised clustering. This new dataset contained 49 patient muscle biopsies analyzed on HG-U133 plus 2.0 microarrays. Samples studied were 6 normal volunteers, 17 DMD, 11 BMD, 7 LGMD2I (limb girdle muscular dystrophy type 2I; FKRP [fukutin-related protein deficiency]), and 8 LGMD2B.

Unsupervised clustering using the 56 network members from Fig. 1 resulted in clustering of the 49 biopsies into two distinct groups indicated by the dendrogram at the top (Fig. 1, purple left group with uniform down-regulation of transcripts and blue right group with uniform up-regulation; and Fig. 2). The two branches did not correspond well to clinical/molecular diagnosis, with Becker, Duchenne, FKRP-deficient and dysferlin-deficient patients seen in both groups. To test whether the segregation of groups was caused by histopathology of the

Published October 13, 2014

Table 1. **List of the 56 transcript genes in the TGF-β network**

Gene	Probe set	P-value	Fold change
ACLY	210337_s_at	0.051	1.125
ASPN	219087_at	<0.001	3.537
BGN	213905_x_at	<0.001	3.717
BMP1	207595_s_at	0.165	1.089
BNIP3L	221478_at	<0.001	1.406
CALD1	212077_at	<0.001	1.767
CAP1	200625_s_at	<0.001	2.218
CAV2	203324_s_at	<0.001	1.76
CFL1	200021_at	<0.001	1.695
CNN3	201445_at	<0.001	2.274
COL1A1	202310_s_at	<0.001	5.386
COL1A2	202404_s_at	<0.001	4.89
COL3A1	211161_s_at	<0.001	3.387
COL4A1	211981_at	<0.001	2.469
COL4A2	211966_at	<0.001	2.762
COL5A1	212489_at	<0.001	2.58
COL5A2	221729_at	<0.001	3.379
COL6A1	213428_s_at	<0.001	2.045
COL6A2	209156_s_at	<0.001	2.251
COL6A3	201438_at	<0.001	2.131
COLEC12	221019_s_at	<0.001	2.363
CSRP2	207030_s_at	<0.001	1.524
CUGBP2	202158_s_at	<0.001	1.537
CYB561	209163_at	<0.001	1.27
DAB2	201280_s_at	<0.001	2.385
ECGF1	204858_s_at	<0.001	2.037
EMILIN1	204163_at	<0.01	2.002
ENG	201809_s_at	<0.001	1.441
HIF1A	200989_at	<0.001	1.981
IFI30	201422_at	<0.001	1.886
JAG1	209098_s_at	<0.001	1.458
KDELR2	200699_at	<0.001	1.361
LOX	215446_s_at	<0.001	2.516
LOXL1	203570_at	<0.001	2.013
LOXL2	202998_s_at	<0.001	1.744
LTBP3	219922_s_at	<0.001	1.507
PGCP	208454_s_at	<0.01	1.237
PGRMC1	201121_s_at	<0.001	1.495
PLOD2	202620_s_at	<0.001	1.725
PLS3	201215_at	<0.001	1.59
RASSF1	204346_s_at	<0.05	−1.163
RSU1	201980_s_at	<0.001	1.522
S100A11	200660_at	<0.001	2.888
SDC2	212158_at	0.269	1.132
SDC3	202898_at	<0.001	2.136
SDCBP	200958_s_at	<0.001	1.408
SERPINH1	207714_s_at	<0.001	1.73
SPARC	200665_s_at	<0.001	2.205
TAX1BP3	209154_at	<0.001	1.64
TBCD	211052_s_at	<0.001	1.581
TGFB1	203085_s_at	<0.001	2.626
TGFBI	201506_at	<0.001	1.852
TGFBR2	208944_at	<0.001	1.852
TGFBR3	204731_at	0.065	1.213
TPM4	209344_at	<0.001	2.086
TUBB2A	204141_at	<0.001	2.16

List of the 56 transcript genes in the TGF-β network (Fig. 1 A) and their fold changes and p-values of *t* test for testing the significance of their changes between two groups: up-regulated group (DMD, JDM, and ED-D) and down-regulated group (FSH, NHM, and ALS). The results shown were from the data processed with PLIER. Those few transcripts showing nonsignificant p-values here are included, as they met significance thresholds with dCHIP mismatch probe set algorithm (not depicted).

muscle studied, the archived interpretation of the severity of the dystrophy was accessed (all read by the same author, E.P. Hoffman; Fig. 2, normal, mild, moderate, or severe dystrophy groups). Mild was defined by evidence of degeneration and regeneration but little or no fibrosis or inflammation. Moderate showed increased inflammation and fiber size variation but minimal or moderate fibrosis. Severe showed fibrofatty replacement of muscle and evidence of failed regeneration. Normal or mild pathology was seen in 20/22 patients in the left branch but only 3/27 in the right branch. In contrast, moderate or severe pathology was seen in 2/22 patients in the left branch and 24/27 in the right branch. Thus, we concluded that this cluster and associated networks were more reflective of severity of histological pathology than clinical/molecular diagnosis.

Query of the putative failed regeneration network in normal staged tissue regeneration identifies time-resolved subnetworks

In many respects, the identification of the TGF-β/fibrosis network was quite expected, as fibrosis is associated with end-stage tissue pathology and with failed regeneration in many tissues, including muscle. However, the majority of patient muscle biopsies were studied at initial diagnosis, before end-stage clinical disease. Moreover, there is increasing evidence that TGF-β is important for normal staged muscle regeneration (Philippou et al., 2008; Kollias and McDermott, 2008; MacDonald and Cohn, 2012). To query the relationship of this cluster with normal regeneration, we overlaid these network members over our previously published 27–time point murine in vivo muscle degeneration/regeneration time series (Fig. 3; Zhao et al., 2003, 2006; Zhao and Hoffman, 2004).

All network members for which we could identify cross-species transcript units and probe sets did indeed show significant regulation of these transcripts in normal regeneration both by heat map (Fig. 3 A) and by statistical comparisons (Table 2). However, we noted from the heat map (Fig. 3 B) that different members of this pathology-associated network were expressed at different time points during normal regeneration. To visualize this temporal-specific pattern, we grouped the 27–time point murine series into four time frames corresponding to relatively distinct periods of muscle regeneration (myoblast proliferation—days 1–3; myotube formation—days 3.5–4.5; myofiber maturation—days 4.5–14; late-stage adaptation—days 20–40; Fig. 3 B). This parsed the TGF-β network in Fig. 1 B into a series of time-resolved subnetworks shown in Fig. 3 B, where the relative expression levels were again coded by both symbol size and color intensity within each subnetwork. The extracellular matrix components commonly associated with pathological fibrosis were seen in the myofiber maturation stage but not other stages.

This analysis evoked a novel hypothesis regarding the distinction between successful regeneration and unsuccessful remodeling (fibrosis). We reasoned that normal regeneration is synchronous, with specific pathways and pathway members having appropriate temporal expression patterns during the 2–3-wk muscle regeneration process. In contrast, dystrophic

Published October 13, 2014

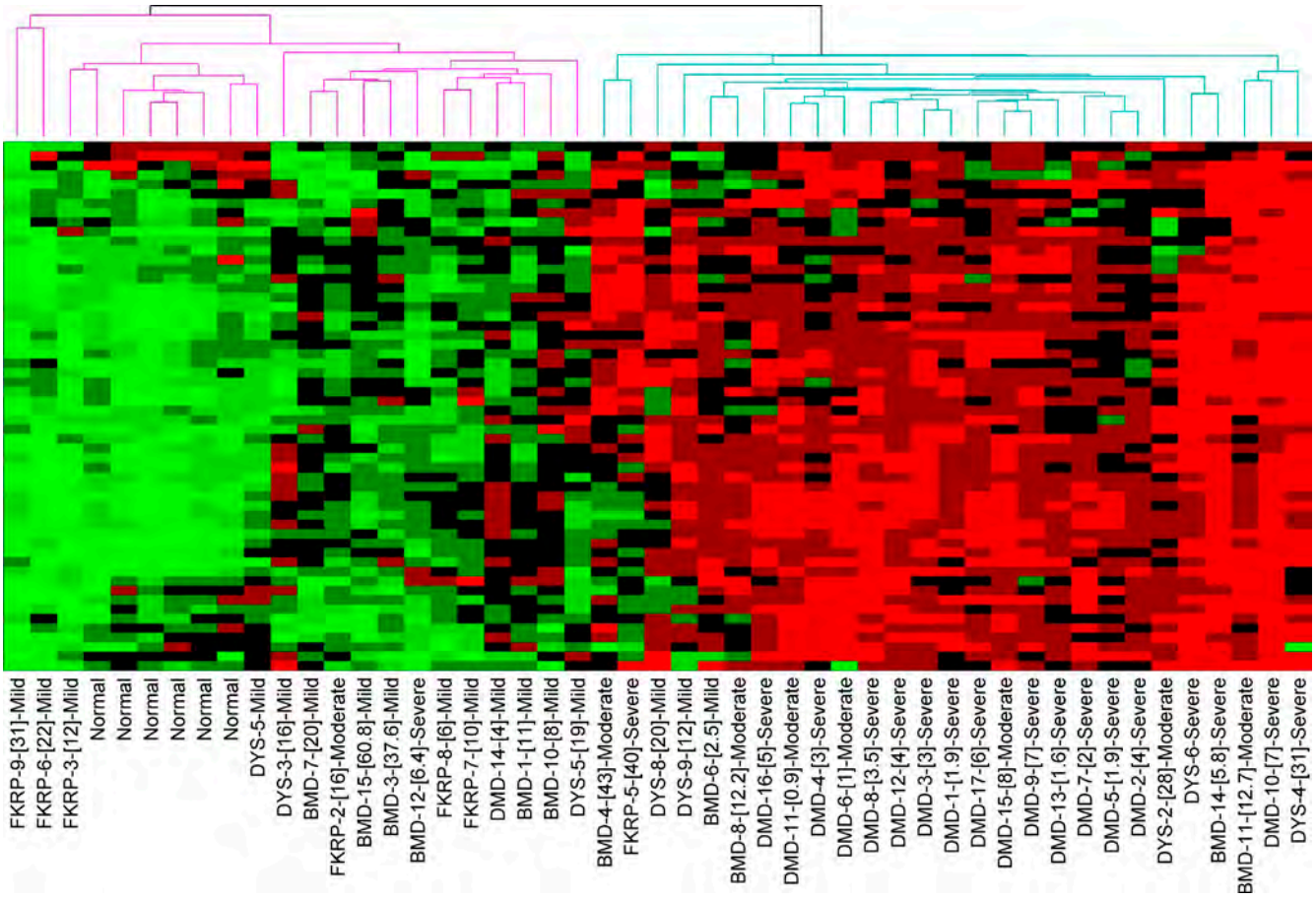

Figure 2. **Unsupervised (blinded) clustering of individual muscle biopsies from a 49-biopsy validation mRNA profiling dataset.** Shown is a heat map using the same 56-member TGF-β network from Fig. 1 B, with visualization of unsupervised clustering of individual biopsies. The specific mRNAs are on the y axis (not depicted), with individual patient biopsies on the x axis (diagnosis, patient number, [age at biopsy], and blinded classification of severity of the histology [normal, mild, moderate, and severe]). The heat map shows bimodal stratification of biopsies (two branches of dendrogram at the top), with the right branch clustering those biopsies with high levels of all or most of these transcripts, whereas the left branch shows lower levels of these transcripts. This clustering is seen to be driven by the severity of the pathology and not patient diagnosis or age (right branch, moderate or severe dystrophic pathology; left branch, normal or mild dystrophic pathology).

muscle was an asynchronous remodeling process, with different regions of the small muscle biopsy studied in different stages of regeneration.

This analysis established the hypothetical model in which asynchronous remodeling may be the driver for failed regeneration, muscle wasting, and early death in the severe dystrophies. By this model, the complete TGF-β–centered network shown in Fig. 1 is only possible in dystrophic muscle. In normal muscle, it is parsed into subnetworks resolved by time. We then sought to test this model experimentally.

Establishing a model of asynchronous muscle regeneration

We reasoned that a potential experimental model to test asynchronous regeneration would be to induce localized regions of muscle degeneration/regeneration in WT mice, with repetitive regional injuries in close proximity within the muscle at defined time points. The experimental design is shown in Fig. S2. In brief, low doses of notexin (10 µl notexin at 5 mg/µl) were injected intramuscularly along with a blue tattoo dye. At a defined time point later, a second injection was performed with the same low dose of notexin, using a red tattoo dye. Mice were sacrificed 13 d after the second injection, a time point when regeneration should be largely complete for both areas. We then focused on specific areas of the muscle, where both injection sites were separated by a relatively small area (50–300 myofibers)—the hypothesis being that myofibers in the microenvironments immediately at the injection sites would be synchronously regenerating, whereas the myofibers in between the two injection sites would receive regeneration cues from both sites (cross talk microenvironment).

In an initial experiment, injections were spaced by 0 (two injections at the same time), 1, 2, 4, 5, and 10 d (four muscles at each time point). Cryosections from the belly of each muscle were analyzed for fibrotic content (Fig. S3 A). This analysis showed that increasing time between injections resulted in increasing content of fibrosis of the muscle (Fig. S3 A). This suggested that the timing of injections influenced the amount of fibrotic tissue deposited in the muscle as a whole tissue.

We hypothesized that asynchronous remodeling may result from interference in intercellular signaling when two nearby groups of myofibers are at different stages of regeneration.

Published October 13, 2014

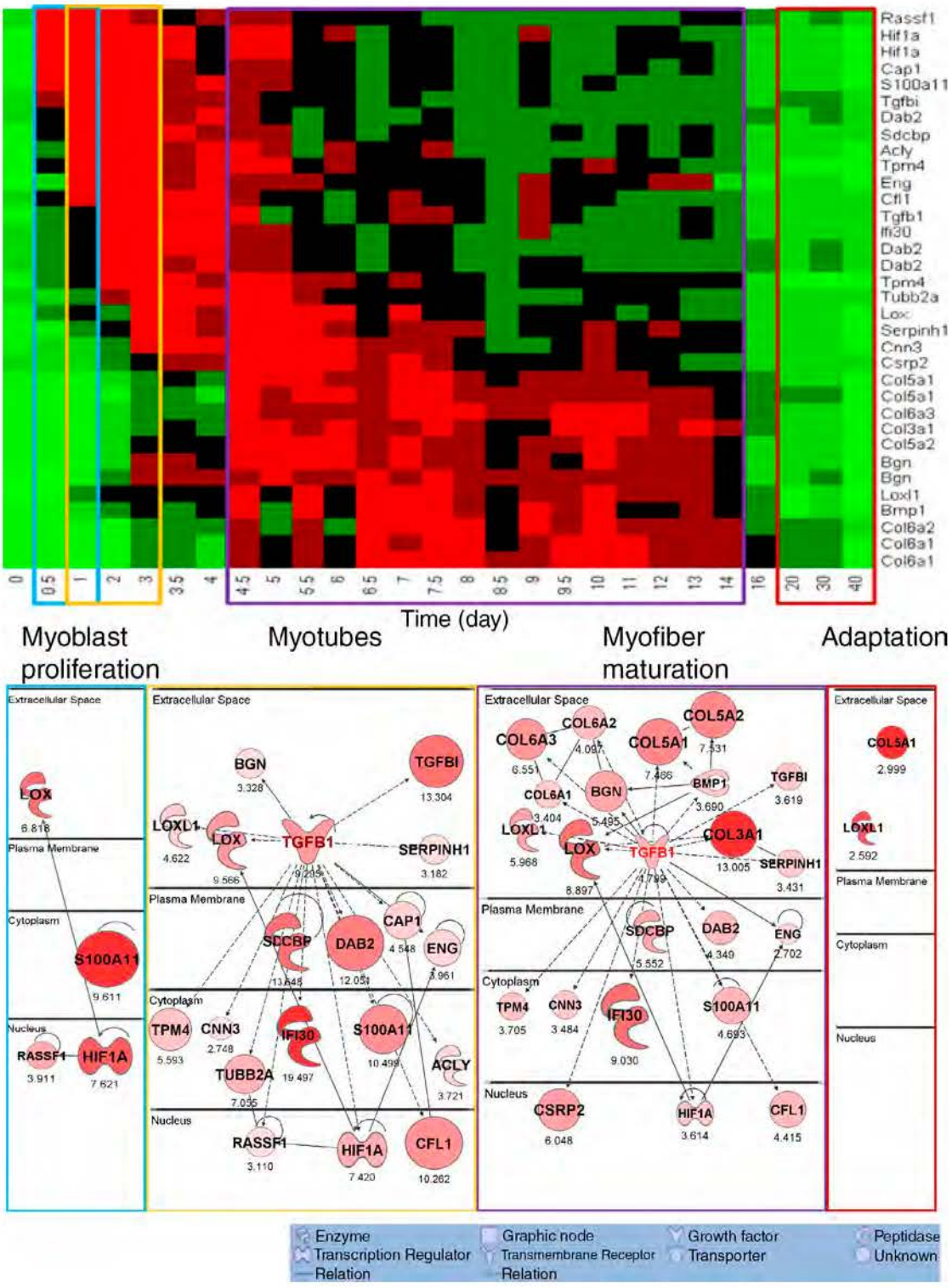

Figure 3. **The TGF-β network superimposed on normal mouse muscle regeneration shows strong induction of subsets of the network at specific time frames during regeneration.** The components of the human TGF-β network (Fig. 1 B) were cross-mapped to the mouse genome and queried in a 27–time point muscle regeneration mRNA profiling dataset (Zhao et al., 2003). The top shows heat map visualization, with network members listed on the right y axis, and the time points after regeneration are shown on the x axis (days). Each member of the TGF-β network shows up-regulation within certain stages of normal staged muscle regeneration, although these stages vary depending on the specific network member. The time points are shown grouped (colored boxes) into early myoblast proliferation stage (blue box), myotube stage (yellow box), myofiber maturation stage (purple box), and late myofiber adaptation stage (red box). The transcripts showing up-regulation within each of these stages of regeneration were then used to generate networks (bottom). This shows that the TGF-β network seen in muscular dystrophy muscle (Fig. 1 B) is parsed into subnetworks based upon the stage of normal regeneration that the subset of transcripts is expressed. Numbers indicate fold change. Statistical data associated with this network and heat map visualization are provided in Table 2.

Published October 13, 2014

Table 2. **The subset of genes of TGF-β network significantly up-regulated in each of the four stages in the normal muscle regeneration process and the *t* test results**

Gene	Probe set	P-value	Fold change
0.5–1 d vs. control			
Hif1a	98628_f_at	<0.01	7.576
Hif1a	98629_f_at	<0.01	7.666
Lox	160095_at	<0.05	6.818
Rassf1	102379_at	<0.01	3.911
S100a11	98600_at	<0.05	9.611
1–3 d vs. control			
Acly	160207_at	<0.001	3.721
Bgn	162347_f_at	<0.01	3.643
Bgn	96049_at	<0.01	3.013
Cap1	93721_at	<0.001	4.548
Cfl1	99119_at	<0.001	10.262
Cnn3	160150_f_at	<0.05	2.748
Dab2	104633_at	<0.01	9.586
Dab2	98044_at	<0.01	4.343
Dab2	98045_s_at	<0.001	22.223
Eng	100134_at	<0.001	3.961
Hif1a	98628_f_at	<0.001	7.293
Hif1a	98629_f_at	<0.001	7.546
Ifi30	97444_at	<0.01	19.497
Lox	160095_at	<0.01	9.566
Loxl1	103850_at	<0.001	4.622
Rassf1	102379_at	<0.01	3.11
S100a11	98600_at	<0.001	10.499
Sdcbp	93017_at	<0.001	13.648
Serpinh1	94817_at	<0.01	3.182
Tgfb1	101918_at	<0.01	9.295
Tgfbi	92877_at	<0.001	13.304
Tpm4	95542_at	<0.001	5.322
Tpm4	95543_at	<0.001	5.865
Tubb2a	94835_f_at	<0.01	7.055
4.5–14 d vs. control			
Bgn	162347_f_at	<0.001	6.38
Bgn	96049_at	<0.01	4.61
Bmp1	92701_at	<0.001	3.69
Cfl1	99119_at	<0.001	4.415
Cnn3	160150_f_at	<0.001	3.484
Col3a1	102990_at	<0.001	13.005
Col5a1	101080_at	<0.001	10.476
Col5a1	93472_at	<0.001	4.456
Col5a2	92567_at	<0.001	7.531
Col6a1	162459_f_at	<0.001	3.744
Col6a1	95493_at	<0.01	3.064
Col6a2	93517_at	<0.001	4.097
Col6a3	101110_at	<0.01	6.551
Csrp2	93550_at	<0.001	6.048
Dab2	104633_at	<0.001	3.517
Dab2	98045_s_at	<0.001	5.182
Eng	100134_at	<0.001	2.702
Hif1a	98628_f_at	<0.001	3.57
Hif1a	98629_f_at	<0.001	3.659
Ifi30	97444_at	<0.001	9.03
Lox	160095_at	<0.001	8.897
Loxl1	103850_at	<0.001	5.968
S100a11	98600_at	<0.001	4.693
Sdcbp	93017_at	<0.001	5.552
Serpinh1	94817_at	<0.05	3.431
Tgfb1	101918_at	<0.01	4.799
Tgfbi	92877_at	<0.001	3.619
Tpm4	95542_at	<0.001	3.229
Tpm4	95543_at	<0.001	4.181
Tubb2a	94835_f_at	<0.001	4.807
20–40 d vs. control			
Col5a1	101080_at	<0.01	2.999
Loxl1	103850_at	<0.01	2.592

To test this, we used laser capture microscopy (LCM) to collect groups of myofibers at the sites of injury, as identified by red and blue tattoo dyes, and the myofibers in between the sites of injury. We focused on the mouse groups of 0, 4, and 10 d between injections.

Five regions were excised using LCM from each muscle: (1) blue dye area (injection 1; 17 d after injection for 4-d series and 23 d after injection for 10-d series), (2) red dye area (injection 2; 13 d after injection for both series), (3) muscle fibers in between the two injections sites (called in-between), (4) normal nonregenerating (intact) myofibers (identified by peripheral nuclei), and (5) single regeneration site (single dye area with no evidence of the second dye). These areas were identified by centralized nuclei myofibers located in the external area of one injury site (either blue or red).

LCM-excised regions were used for mRNA isolation and mRNA profiling using Illumina bead arrays. Unsupervised chip clustering showed excellent signal/noise balance, as indicated by the clustering of microarray replicates of LCM from adjacent muscle sections (Fig. S2 C). For data analysis, we first compared region 4 (uninjured) versus region 5 (single regeneration). There were very few differentially regulated transcripts, suggesting that the muscle in region 5 had indeed successfully regenerated to completion. Likewise, there were few statistically significant differences between region 1 (first injury) versus region 5 and region 2 (second injury) versus region 5 (single site), consistent with successful remodeling (unpublished data).

In contrast, comparison of the tissue in-between injuries (area 3) showed mRNA expression profiles that were quite distinct from neighboring regions and also remarkably different for the 4-d series (Fig. 4) versus the 10-d multiinjury series (Fig. 5). Specifically, the 4-d in-between myofiber region showed a relative loss of mitochondrial-related transcripts and an increase in inflammatory transcripts (Fig. 4, left). The 10-d in-between myofiber region showed increase of extracellular matrix components (Fig. 5, left). Statistical comparison of fold changes and p-values between the 4- and 10-d multiple injection sites showed highly significant differences, with the mitochondrial changes specific to the 4-d time series (Table 3) and the extracellular matrix transcripts specific to the 10-d time series (Table 4). Alignment of the

Published October 13, 2014

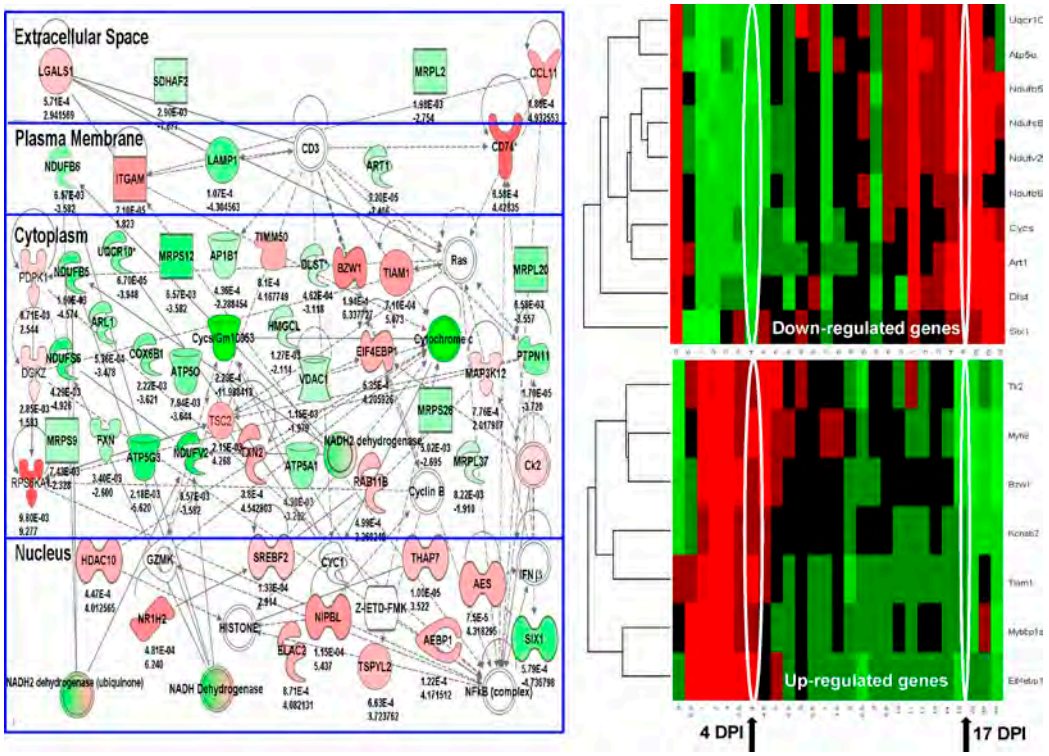

Figure 4. **Muscle tissue areas located between asynchronous injuries spaced 4 d apart show chronic inflammation and loss of mitochondrial transcripts.** LCM was used to isolate regions of myofibers in between injury sites (cross talk area) spaced 4 d apart, with muscles studied 13 d after the second injection when myofiber regeneration was expected to be largely complete. Shown is the top-ranked Ingenuity network (left) reflective of chronic inflammation (red gene/protein symbols), and loss of mitochondrial components (green symbols). This network was then superimposed on normal murine regeneration time series (right), separated by the mitochondrial-related transcripts (down-regulated genes; top right) and inflammatory transcripts (up-regulated genes; bottom right). The mice that were sacrificed after regeneration should be largely complete (17 d postinjection [DPI]). However, the myofibers between the two injury sites showed expression patterns that were more consistent with the 4-d time point (4 d postinjection). Statistical analyses associated with the heat map are provided in Table 4. These data suggest that the myofibers in between the two injury sites are suspended in a time period of regeneration, defined by the days between the two sequential injuries (cross talk microenvironment). Numbers indicate p-value (top) and fold change (bottom).

subcellular localizations of the components of the top-ranked Ingenuity networks for the 4 and 10 d confirmed the preponderance of intracellular protein changes in the 4 d, in contrast to the extracellular matrix components in the 10 d (Fig. S3, B and C).

We then overlaid the gene networks in Fig. 4 over normal staged muscle regeneration, separating the up-regulated and down-regulated transcripts (Fig. 4, right). This showed that the down-regulated mitochondrial transcripts were highly expressed in uninjured and fully regenerated muscle but were strongly down-regulated both in the 4-d in-between area as well as the 4-d time point during normal staged regeneration. This was consistent with the myofibers in between the two injury sites having suspended regeneration at the 4-d time point. Similarly, the up-regulated inflammatory transcripts in the in-between area separated by 4 d were highly expressed at the 4-d time point of normal staged regeneration but not at the later fully regenerated time point (Fig. 4). Thus, both the down-regulated mitochondrial transcripts and the up-regulated inflammatory transcripts in the in-between area appeared arrested at the time point separating the asynchronous injury times.

The 10-d staged injury series was also consistent with the suspended development model. Connective tissue remodeling transcripts were highly up-regulated in the in-between area separated by 10 d, and this pattern was consistent with the 10-d time point in normal regeneration (Fig. 5, right). Statistical analysis showed that this pattern was largely specific to the 10-d staged remodeling and not seen in the 4-d staged remodeling (Table 4).

The microarray data from the 10-d interval injury model showed that the myofiber region in between asynchronous injuries showed inappropriate persistent expression of connective tissue-remodeling transcripts, and this would be consistent with the pathological findings of localized tissue fibrosis. Although we had previously shown an overall increase in fibrosis that was highest in the day 10 staged series muscle (Fig. 3 A), we refined this analysis to the localized area in between the two injection sites (Fig. 6). Histological visualization of the area between the two injection sites showed dramatic fibrotic replacement of muscle in the 10-d series, which was not seen with the 0- and 4-d series (Fig. 6).

Targeted experiments confirm aberrant expression of fibrotic transcripts (10 d apart) and persistent inflammation and loss of mitochondrial capacity (4 d apart)

To validate the mRNA microarray findings, we selected specific transcripts and proteins to evaluate using an independent series of mice that had been subjected to the same 4- and 10-d asynchronous muscle injuries. Tattoo dyes were used to visualize the

Published October 13, 2014

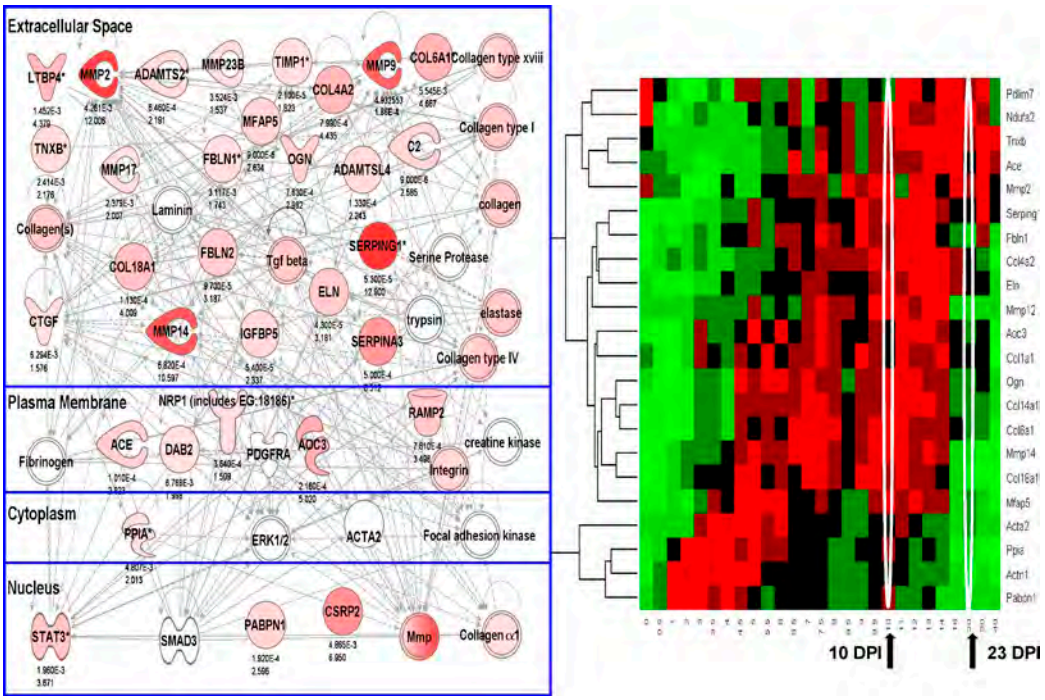

Figure 5. **Muscle tissue areas located between asynchronous injuries spaced 10 d apart show a high level expression of profibrotic gene networks.** Shown is data for the LCM region of muscle between the two injury sites spaced 10 d apart. The myofibers between the two injury sites show a high level expression of transcripts associated with connective tissue proliferation and fibrosis (top-ranked Ingenuity network, left). Superimposing this network on normal staged murine regeneration shows that the myofibers in the area between the two injury sites show expression patterns consistent with suspension in the 10-d time point of normal regeneration. Statistical analyses associated with the heat map are provided in Table 4. Numbers indicate p-value (top) and fold change (bottom). DPI, day postinjection.

Table 3. **Down-regulated metabolic gene transcripts are shared between 3 and 4 d of synchronous regeneration and 4-d asynchronous remodeling**

Genes	P-value/FC							
	27–time point single regeneration series				Double injection LCM series			
					4 d between injections		10 d between injections	
	3/4 d[a]	9/10 d[a]	13/14 d[a]	30/40 d[a]	Single site[b]	In-between[b]	Single site[b]	In-between[b]
ATP5A1 100753_at	0.06	NS	NS	NS	NS	0.004/−3.27	NS	NS
COX6B1 99114_r_at	0.01	NS	NS	NS	NS	0.002/−3.62	NS	NS
CYCS 98132_at	0.06	NS	NS	NS	NS	0.0002/−12	NS	NS
NDUFB5 97307_f_at	0.002	0.05	0.05	0.04	NS	0.001/−4.6	NS	0.002/−2.5
UQCRC1 101989_at	0.07	NS	NS	NS	NS	0.009/2.6	NS	NS
ART1 104638_at	0.02	NS	NS	NS	NS	0.00009/−2.4	NS	NS
ARL1 97505_at	0.02	NS	NS	NS	NS	0.0005/−3.5	NS	NS
MRPS12 98547_at	0.02	NS	NS	0.04	NS	0.0006/−5.4	NS	NS
MRLP20 94875_at	0.01	NS	NS	NS	NS	0.006/−3.6	NS	NS

The nine mRNA transcripts shown were significantly down-regulated in the region between asynchronous injection sites in the double LCM series when injections were separated by 4 d, but not 10 d (8/9). In a separate 27–time point synchronous regeneration time series, these same transcripts were down-regulated at the 3–4-d time point and not later time points. FC, fold change.
[a]Days are versus 0.
[b]Sites are versus nonregenerating.

Published October 13, 2014

Table 4. **Up-regulated fibrosis-associated gene transcripts are shared between 9 and 14 d of synchronous regeneration and 10-d asynchronous remodeling**

Genes	P-value/FC							
	27–time point single regeneration series				Double injection LCM series			
					4 d between injections		10 d between injections	
	3/4 d[a]	9/10 d[a]	13/14 d[a]	30/40 d[a]	Single site[b]	In-between[b]	Single site[b]	In-between[b]
ACTA2 93100_at	0.001	0.006	0.002	NS	NS	0.005/8.3	NS	0.008/16.8
COL6A1 95493_at	0.003	0.0001	0.0001	0.02	NS	0.002/−3.6	NS	0.00004/7.2
COL18A1 101039_at	0.00001	0.0003	0.01	NS	NS	NS	NS	0.0001/4.0
COL4A2 101039_at	NS	0.01	0.008	NS	NS	NS	NS	0.0007/4.5
ELN 92207_at	NS	0.004	0.02	NS	NS	NS	NS	0.00004/3.2
MMP14 160118_at	0.0007	0.0002	0.006	NS	NS	NS	NS	0.0006/10.6
COL14A1 99476_at	0.007	0.004	0.002	NS	NS	NS	NS	0.0003/1.5
COL15A1 99637_at	0.02	NS	0.006	NS	NS	NS	NS	0.004/1.6
C2 103673_at	0.02	0.02	NS	NS	NS	NS	NS	0.000009/2.6
STAT3 99099_at	0.02	0.002	0.05	NS	NS	NS	NS	0.003/4.4
CDKNA1 94881_at	0.03	0.05	0.009	NS	NS	NS	NS	0.00007/3.25
RAMP2 994444_at	NS	0.007	0.006	NS	NS	NS	NS	0.0007/3.5
ACVR2B 994444_at	NS	0.007	0.006	NS	NS	NS	NS	0.0004/6.45

The 13 gene transcripts shown were significantly up-regulated in the region between asynchronous injection sites in the double LCM series when injections were separated by 10 d, but not 4 d (0/13). In the 27–time point synchronous regeneration time series, these same transcripts showed the highest and consistent up-regulated between 9 and14 d. FC, fold change.
[a]Days are versus 0.
[b]Sites are versus nonregenerating.

first and second injection sites. Tissue for quantitative RT-PCR (qRT-PCR) was obtained by LCM. Immunohistochemistry and enzyme histochemistry were also performed.

The 4-d interval injury model showed an increase in inflammatory transcripts and a relative loss of mitochondrial-associated transcripts (Fig. 4). qRT-PCR confirmed the mRNA profiling data, showing preferential loss of mitochondrial transcripts in the region in between the two injections sites, relative to other regions of the same muscle tissue and the area between two notexin injections made on the same day (Table 5). To confirm the relative loss of mitochondrial oxidative capacity predicted by expression microarray and qRT-PCR microarray data for the 4-d in-between areas, we used standard enzyme histochemistry (NADH, cytochrome *c* oxidase [COX], succinate dehydrogenase [SDH], and a combination of NADH and COX enzymatic staining). The region between the 4-d interval injection sites showed a relative loss of mitochondrial enzymatic activity stains compared with other injection paradigms, confirming the microarray data (Fig. S4).

To validate the up-regulation of proinflammatory transcripts, we studied three proteins by immunofluorescence localizations in three double injury mice (injuries spaced 0, 4, and 10 d apart; CD11b, CD74, and CD163; Fig. 7). These proteins were selected based on their role in proinflammatory pathways as well as DMD pathogenesis. CD11b is a leukocyte marker that induces innate immune response resulting in phagocytosis and cell-mediated cytotoxicity (Solovjov et al., 2005). CD11b immunostains showed the highest expression in the in-between region at 4 d but not 10 d or the simultaneous injection control (Fig. 7 A).

Human leukocyte antigen class II histocompatibility antigen γ chain (CD74) was selected because of its role in regulating adaptive immune response upon injury and its induction of NFK-β pathways (one of the earliest proinflammatory markers of DMD; Cresswell, 1994; Chen et al., 2005). CD74 showed mRNA up-regulation in the 4-d between area and not the 10-d area (Fig. 4 and Table 3). Immunostaining of CD74 showed expression in the region between the 4-d injection sites but not the region in between the 10-d injection sites (Fig. 7 B). CD74 was also not seen in the injection sites themselves.

CD163 is a marker of specific macrophage subtypes (M2c) in dystrophin-deficient muscles, is associated with increased tissue repair (Villalta et al., 2009), and is a known acute phase-regulated receptor (Madsen et al., 2001). The immunostaining

Published October 13, 2014

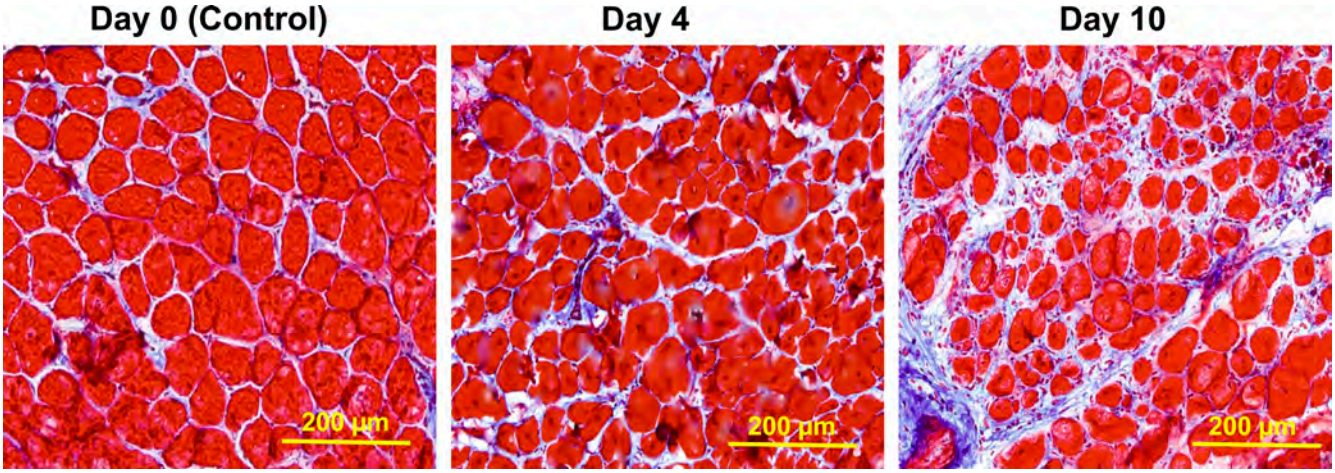

Figure 6. **Histological analysis of connective tissue proliferation (fibrosis).** Shown is Masson's modified trichrome staining of cryosections in the area of muscle between injection sites staged 0, 4, and 10 d apart (n = 3 muscles per group). Endomysial fibrosis is most evident in the area between injections space 10 d apart, consistent with the LCM expression profiling data (Fig. 4 B).

patterns for CD163, cell surface markers of monocytes and macrophages class II (M2c), showed similar patterns (Fig. 7 C).

For the 10-d interval injuries, we had shown increases in connective tissue by histological methods (Fig. 6 and Fig. S3 A). To further validate this finding by immunostaining of specific proteins, CD206 (MRC1 [mannose receptor, C type 1]; macrophage marker) and MMP9 (metalloproteinase implicated in dystrophy pathogenesis; Dahiya et al., 2011a,b; Miyazaki et al., 2011) were studied (Fig. 8). Both showed strong expression of the myofiber in-between region of injuries spaced 10 d apart, with lack of immunostaining in 4-d injuries or 0-d control.

LCM of human DMD patient muscle shows patterns consistent with asynchronous remodeling

Muscle biopsies from DMD patients have long been recognized to show grouped degeneration and regeneration and focal fibrosis. This histological pattern is consistent with the asynchronous remodeling shown in our murine experimental model. To provide evidence for asynchronous remodeling in human DMD muscle at the molecular level, we studied a frozen diagnostic muscle biopsy from a young child with DMD (3 yr). Frozen sections were stained by hematoxylin and eosin to identify neighboring regions of myofibers both within fascicles and between fascicles (Fig. 9 A), and different subregions (1–6) were identified and then isolated by LCM and subjected to Illumina mRNA profiling. Histochemical staining for mitochondrial enzyme function showed the variable loss of mitochondrial oxidative phosphorylation activity typically seen in DMD biopsies (Fig. 9 B). There were variable degrees of inflammation and fibrosis, as detected by Masson's trichrome and Gomori's trichrome (Fig. 9, C and D). Unsupervised clustering of the microarrays from adjacent sections showed clear and consistent differences in expression profiles from the six regions, with replicates of profiles clustering together, yet each region showing a distinct pattern from other regions.

As we were unable to specifically stage the pathology of the human biopsy, the specific timing of the degeneration and regeneration cycles of the six regions could not be determined. Nonetheless, the profiles were consistent with asynchronous bouts of degeneration/regeneration leading to chronic inflammation and mitochondrial function loss associated with the murine 4-d spaced multiple injuries and the fibrosis associated with the 10-d multiple injuries.

Pharmacogenomics of glucocorticoids on the proposed intercellular signaling networks

Daily glucocorticoids are considered standard of care in DMD (Bushby et al., 2010). The mechanisms of action of glucocorticoids in DMD are thought to be through antiinflammatory mechanisms as in other chronic inflammatory states (Hoffman et al., 2012).

Table 5. **RT-PCR validation of loss of mitochondrial transcripts in the area between staged degeneration/regeneration cycles 4 d apart**

Genes	P-value/FC		
	Between 4D vs. single injury area	Between 4D vs. intact/uninjured area (same section)	Between 4D vs. between area of the control synchronous mice
Cox6b1	0.0005/−2.6	0.0004/−4.9	0.004/−1.4
Ndufs6	0.003/−3.6	0.04/−16.0	0.001/−6.9
Ndufb5	0.01/−4.9	0.002/−11.0	0.02/−11.0
Ndufb6	0.004/−6.5	0.009/−7.2	0.0002/−20.0

FC, fold change.

Published October 13, 2014

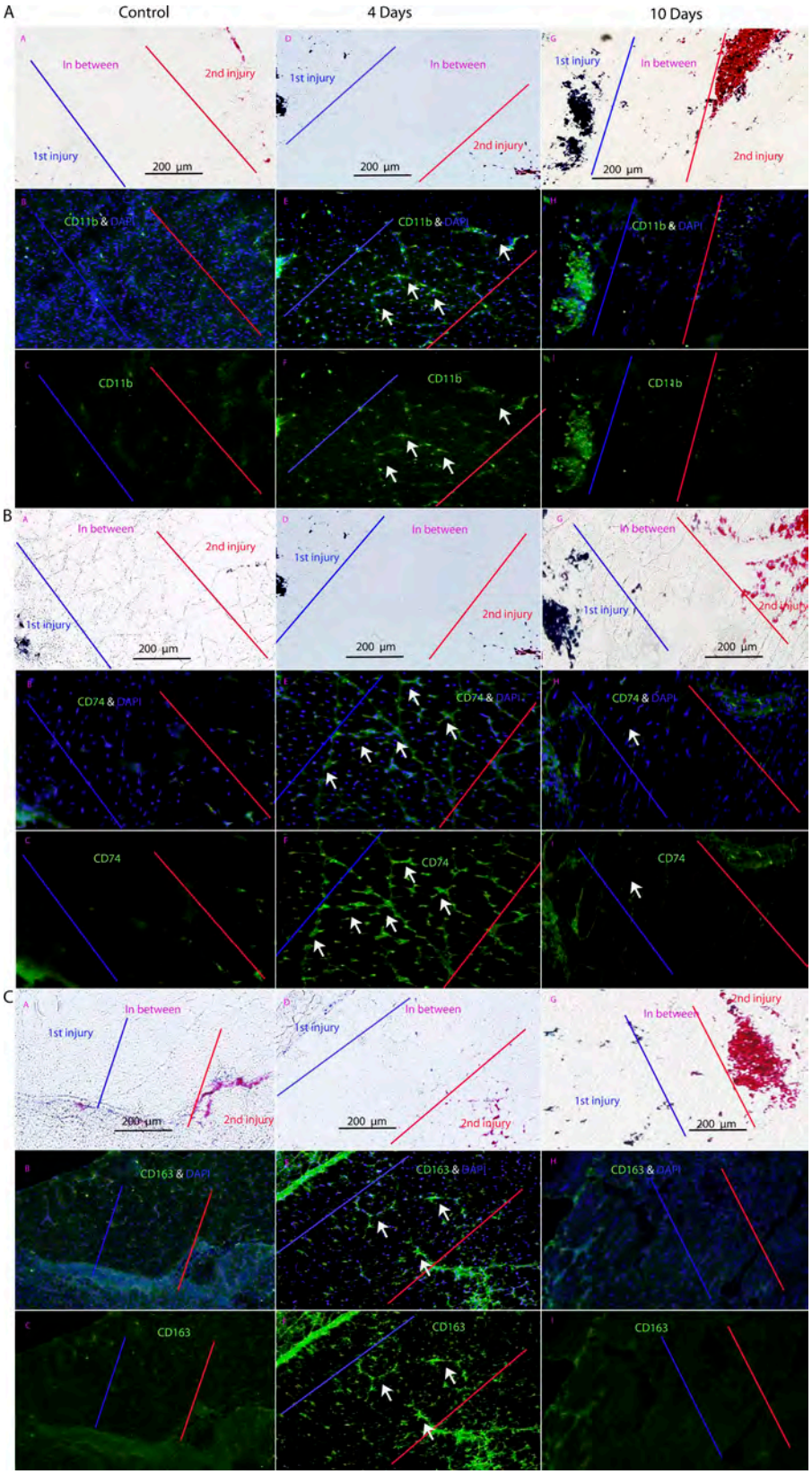

Figure 7. **Immunostaining of inflammatory proteins CD11b, CD74, and CD163 shows expression specific to intervening areas of muscle between injuries spaced 4 d apart.** (A–C) Shown are immunofluorescence stains for inflammatory protein markers CD11b (A), CD74 (B), and CD163 (C). Each panel shows matched phase contrast (marking injury sites with tattoo dyes), antigen with nuclear stains (DAPI), and antigen alone. All three inflammatory markers show preferential localization in the area between the two injury sites only when injuries are spaced 4 d apart and not 0 or 10 d apart (n = 3 muscles per group). Arrows indicate immunoreactive material in the microenvironment between two neighboring sites of regeneration.

However, extensive side effect profiles, such as muscle wasting typically associated with glucocorticoids, and differences in response between human and mouse models have complicated dissection of the molecular mechanism of action (Sali et al., 2012). Recently, we developed a novel dissociative steroid, VBP15, that is similarly antiinflammatory yet lacks most side effects associated with glucocorticoid response element–mediated transactivation subactivities (Heier et al., 2013). We hypothesized

Published October 13, 2014

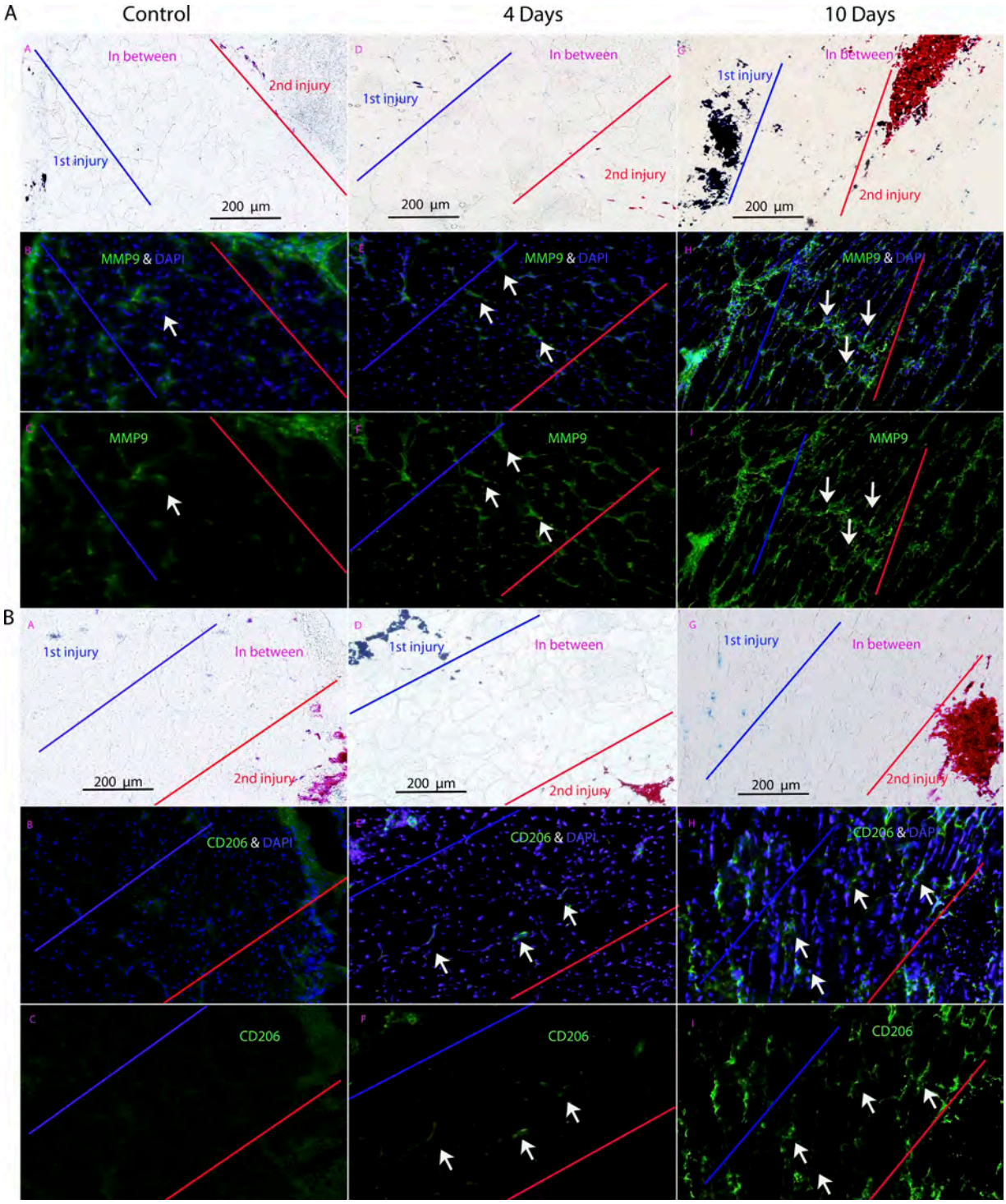

Figure 8. **Immunostaining of proteins profibrotic markers MMP9 and CD206 shows preferential expression the area of muscle between injuries spaced 10 d apart.** (A and B) Two markers associated with fibrosis, MMP9 (A) and CD206 (B), are shown by immunostaining in muscles from repeated injuries (control = 0 d apart; 4 and 10 d apart). Both markers show preferential expression in the area in between the two injury sites when the injuries are spaced 10 d apart and not 0 (control) or 4 d (n = 3 muscle per group). Arrows indicate immunoreactive material in the microenvironment between two neighboring sites of regeneration.

that both prednisone and VBP15 might serve to suppress inappropriate intercellular signaling in the regions between asynchronously injured and remodeling areas of muscle, particularly those associated with the proinflammatory 4-d asynchronous cross talk regions.

We tested the effects of drug treatment on the TGF-β–based asynchronous remodeling networks both in the *mdx* mouse model as well as the WT asynchronous remodeling experimental system. For the *mdx* model, we obtained frozen muscle samples from a previously described preclinical trial of prednisone and

Published October 13, 2014

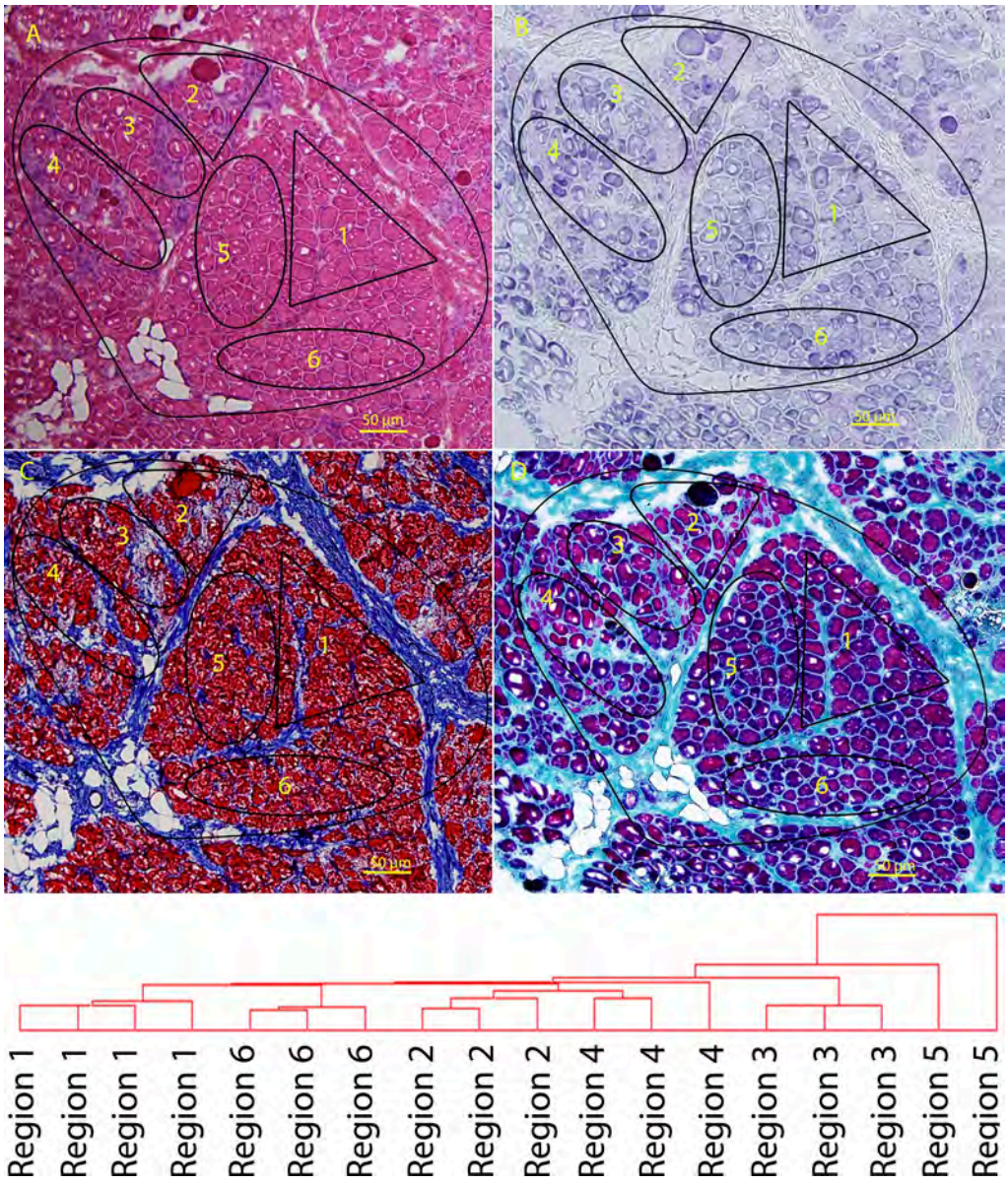

Figure 9. **LCM of regions of a muscle biopsy from a DMD patient.** (A–D) A frozen muscle biopsy from a 3-yr-old DMD patient was stained for hematoxylin and eosin (A), mitochondrial enzyme activity (SDH; B), Masson's modified trichrome (C), and Gomori's modified trichrome (D). Variable states of degeneration and regeneration can be seen within each fascicle. The different regions indicated (1–6) were isolated by LCM, and individual regions ($n \geq 3$ per region) were analyzed by mRNA profiling. The areas were chosen based on visual histopathology, where both fascicles and relatively distinct histological subareas within the fascicles were chosen. Microarray data from replicates of LCM regions microdissected from adjacent cryosections was subjected to unsupervised chip-based clustering. This showed replicates to cluster closely in the dendrogram. This represents heterogeneity within fascicles in DMD muscle, as hypothesized by the asynchronous regeneration model described in the accompanying text.

VBP15 (Heier et al., 2013). Drug treatments were started at 10 wk of age and continued to 26 wk of age (4 mo of treatment). Skeletal muscles (gastrocnemius) of mice treated with 5 mg/kg/d prednisone and 15 mg/kg/d VBP15 were tested by mRNA profiling ($n = 5$ per group) using Illumina bead arrays. As a baseline study, the human TGF-β–centered network, including HIF1A and S100A11 nodes, was queried in untreated *mdx* versus WT mice, and this showed strong up-regulation of the majority of network members (22/29; Fig. 10 A). A marked exception was HIF1A, a key ischemia-responsive gene; however, the rapid expression of HIF1A upon necropsy may lead to postmortem expression in WT animals. Comparing prednisone- and VBP15-treated *mdx* mice with untreated *mdx* mice showed both drugs to significantly down-regulate the majority of the pathway members (15/29 prednisone and 12/29 VBP15), including TGF-β ligand and HIF1A. These data suggest that a possible mechanism of action of both prednisone and VBP15 is through suppression of the TGF-β–related networks, leading to more successful regeneration.

We then used the same data analysis methods for the WT asynchronous remodeling experimental system, similarly determining the effect of drug treatment on expression of the TGF-β network. As a baseline, expression profiles of LCM samples (cross talk area vs. single injury sites) was performed for both 4- and 10-d asynchronous remodeling samples, with both showing

Published October 13, 2014

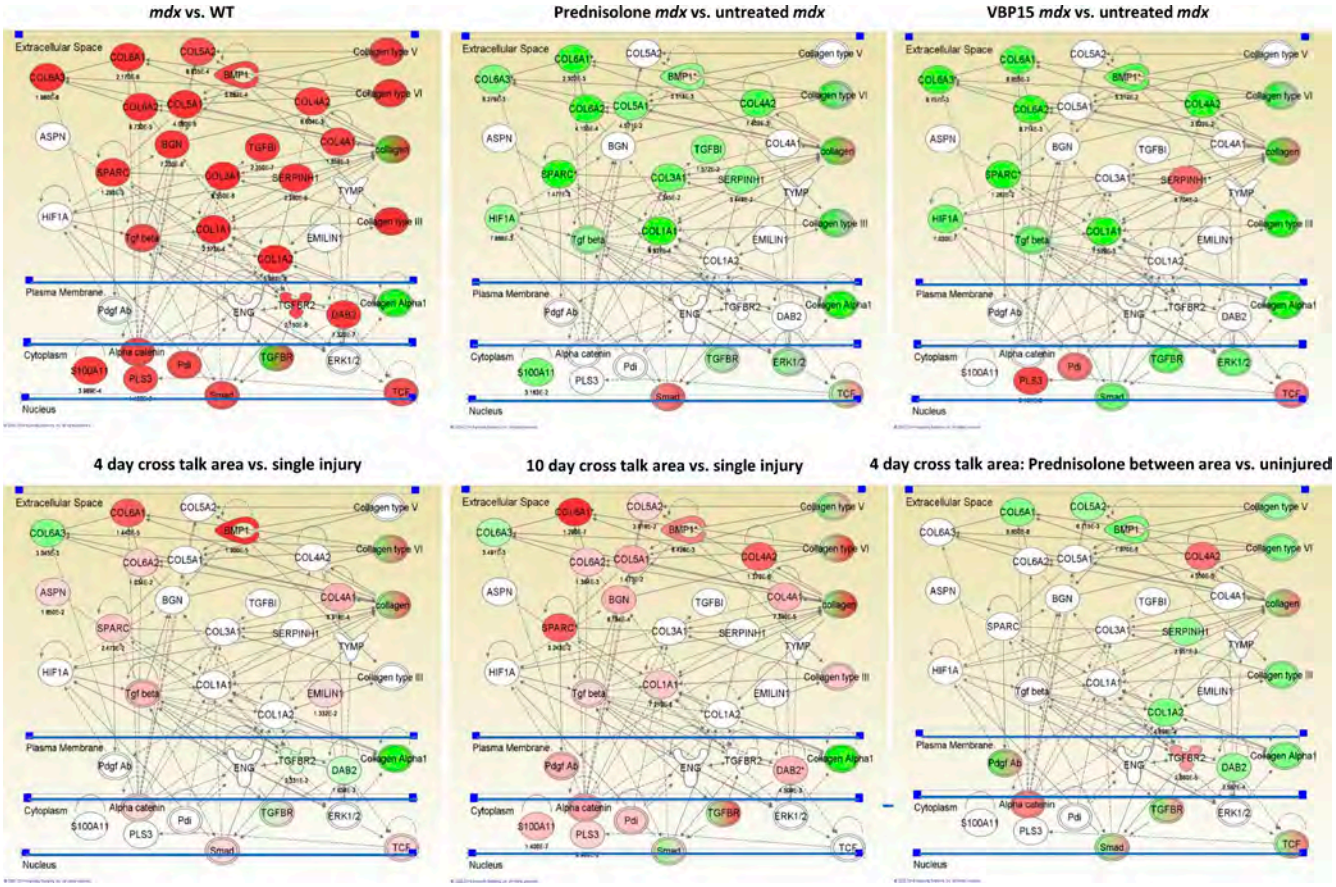

Figure 10. **Treatment with prednisone or VBP15 suppresses the TGF-β network in both WT asynchronous remodeling and *mdx* mice.** Top images are mRNA profile data of skeletal muscles from a 4-mo preclinical drug trial of 5 mg/kg/d prednisone and 15 mg/kg/d VBP15. Muscle functional testing and histology on this trial has been previously published (Heier et al., 2013). The TGF-β and fibrosis pathways seen in experimental asynchronous remodeling and DMD biopsies were queried for the relative expression of mRNAs between the indicated samples, with red color indicating up-regulation (p-values underneath network members) and green color indicating down-regulation. Untreated *mdx* muscle shows strong up-regulation of the network (*mdx* vs. WT). Treatment with either prednisone (prednisone-treated *mdx* vs. untreated *mdx*) or VBP15 (VBP15-treated *mdx* vs. untreated *mdx*) shows strong suppression of this network. Bottom images show comparison of expression profiles from LCM samples of asynchronously remodeling regions of WT muscle. The cross talk region between injection sites shows up-regulation of the TGF-β fibrosis network (higher in 10 d compared with 4 d) and prednisone treatment of 4-d asynchronous remodeling mice with prednisone suppresses the network (pretreated, 4-d cross talk area vs. uninjured).

up-regulation of the TGF-β network in the cross talk microenvironment (10/29 for 4 d and 16/29 for 10 d; Fig. 10). The 10-d cross talk microenvironment showed more extensive up-regulation of the TGF-β networks compared with 4 d, consistent with the findings presented earlier (Fig. 5). Drug treatment of the WT 4-d asynchronous mouse model was performed 1 d before first injury and then continuously during the 13 d after recovery from the second injection (17 d total), using either 5 mg/kg/d prednisone or 15 mg/kg/d VBP15. LCM and mRNA profiling of the cross talk microenvironment was compared with single injury microenvironment in the same muscle. This showed significant down-regulation by prednisone of TGF-β network members in the cross talk region (Fig. 10).

To validate these findings at the immunohistochemical (protein) level, the WT 4-d asynchronous model drug-treated muscles were immunostained for CD11b, CD74, and CD163 and compared with untreated mice. This analysis showed the expected high expression of each protein marker in the 4-d multiple injury sites (Fig. S5). However, daily administration of either prednisolone or VBP15 markedly reduced the immunopositivity for these antigens (Fig. S5). These data are consistent with both glucocorticoids and VBP15 serving to inhibit inappropriate cross talk in asynchronously remodeling muscle.

Discussion

We used a large-scale data integration approach to query the molecular underpinnings of progressive failure of regeneration in the muscular dystrophies (Fig. S1). Using an initial mRNA profiling dataset of 12 disease groups (117 biopsies and 234 microarrays), we developed an iterative composite approach to identify clusters of transcripts that were associated with the more severe muscle disease classes (DMD, JMD, and LMNA; Fig. 1). Functional clustering of the diagnostic transcripts showed a 56-member TGF-β–centered network consistent with tissue fibrosis. Unsupervised clustering of an independent mRNA profiling dataset of 49 biopsies from four muscle disease groups (DMD, BMD, LGMD2I, and LGMD2B) and controls showed a strong correlation of the TGF-β–centered network with pathological

Published October 13, 2014

severity rather than diagnostic criteria (Fig. 2). However, all members of this same 56-gene TGF-β–centered network were expressed during specific stages of normal muscle regeneration, using a 27–time point staged murine regeneration dataset (Fig. 3 A). These data analyses established the hypothesis that normal regeneration and progressive dystrophy involved the same proteins; the only distinction was one of timing and degree of expression. The TGF-β network was parsed into stage-specific subnetworks in normal muscle regeneration yet occurred within the same muscle at the same time in severely dystrophic muscle (Fig. 3 B). We hypothesized that asynchronous bouts of degeneration and regeneration in neighboring regions of muscle tissue could result in inappropriate cross talk between the regions.

To test this hypothesis, we developed an experimental model for asynchronous regeneration of muscle in neighboring microenvironments. An initial injury was induced in normal mouse muscle using notexin with the injection site labeled with tattoo dye. A second adjacent injection, labeled with a second tattoo dye, was subsequently made, at defined times (0–10 d). The mice were sacrificed 13 d after the second injection when regeneration would be expected to be largely complete (Fig. S2). Then, regions of the muscle containing both injection sites and regenerating myofibers in between the sites (cross talk microenvironment) were studied by LCM and in situ immunostaining methods. We found that increasing the time between injections led to a greater degree of abnormal collagen deposition (fibrosis; Fig. S3), indicating that the time period between injections was an important determinant of the response of the muscle to the damage. To better define the response of specific subregions of asynchronously remodeling muscle, we used LCM and mRNA profiling as well as immunostaining, histology, and enzyme chemistry experiments. Myofibers in between the two injury sites showed an expression pattern that seemed suspended within the developmental stage that separated the two injections, with the 4- versus 10-d between staged injections sharing little similarity with each other (Fig. 4 and Fig. S3, B and C). The myofibers between the sites of the 10-d repeat injections showed strong expression of transcripts associated with a profibrotic state, with high expression of collagens, and other connective tissue remodeling networks (Fig. 5). This showed considerable overlap of network members, such as TGF-β, COL1A1, COL4A1, COL4A2, and COL6A1, with the human muscle biopsy TGF-β network associated with fibrosis (Fig. 1 B) and was similar to the myotube maturation subgroup of normal staged (synchronous) muscle regeneration (Fig. 3). To assign statistical support to these visualizations of LCM data networks, we took specific network members (mRNAs) and defined expression changes (p-values and fold changes) in specific time points of regeneration, 4-d in-between LCM data and 10-d in-between LCM data (Table 4). The expression patterns were consistent with inappropriately prolonged and extensive connective tissue remodeling, in which signaling led to suspension of progression through the 10-d time window of normal regeneration. In other words, the tissue region between the injection sites staged 10 d apart remained fixed in the 9–10-d regeneration program and appeared unable to successfully mature past this developmental time point.

Our data showed that normal regeneration and failed regeneration involve the same networks, differences largely being caused by the synchrony (episodic) nature of normal regeneration and the asynchronous (repeated injury) nature of failed regeneration. With failed regeneration, regenerating myofibers are likely receiving incorrect temporal cues from their neighbors, and this inappropriate cross talk leads to inability to progress through the normal temporal stages of regeneration.

Glucocorticoids are derivatives of cortisol, the diurnal hormone that sets day/night cycles in most animals and plants. Pharmacological doses of glucocorticoids, typically given on a daily basis, are considered antiinflammatory and remain among the most effective drugs for chronic inflammatory states since their initial use in the 1940s. There is increasing recognition of the role of cortisol and clock genes in establishing cell cycle regulation throughout the body and that disturbances or blunting of diurnal cortisol fluctuations are associated with the proinflammatory state (Niimi et al., 2007; Holderfield and Hughes, 2008). We recently showed that primary bronchial epithelial cells from asthmatic patients are intrinsically dyssynchronous, are proinflammatory, and poorly repair wounds, yet this can be normalized with pulsed glucocorticoids (Freishtat et al., 2011; Alcala et al., 2014).

We reasoned that the effectiveness of glucocorticoids in DMD may be caused by resynchronization of remodeling, thereby rescuing the inappropriate cross talk described in this paper. To test this, we treated WT mice with prednisolone, VBP15 (a dissociative steroid), and vehicle/placebo and then tested for the drug regimens to rescue the inappropriate cross talk in our asynchronous regeneration model. Drug treatments of both *mdx* mice and the WT asynchronous model were tested (Fig. 10 and Fig. S5). As hypothesized, both prednisolone and VBP15 reduced evidence of cross talk in both *mdx* and the WT asynchronous models. These data suggest that part of the mechanism of action of both prednisone and VBP15 is through suppression of TGF-β networks induced by asynchronous remodeling.

There is an extensive literature supporting many of the findings in our study, although we believe that this study is the first to synthesize these observations into a single model. Specifically, transient TGF-β activity is essential for maintaining normal tissue repair and regeneration, whereas persistent TGF-β activity results in excessive fibrosis and, ultimately, scarring in skin and internal organs. In dystrophic muscle, TGF-β may affect tissue fibrosis by elevating collagen secretion by fibroblasts and converting myoblasts to fibroblasts. Furthermore, TGF-β can inhibit terminal myogenic differentiation and thus impair muscle repair process (Alexakis et al., 2007).

Our model may provide an explanation for the enigmatic pathology of the *mdx* mouse. Dystrophin-deficient mouse muscle shows normal histology in early weeks postpartum (0–3 wk) and then a stage of widespread necrosis followed by relatively successful regeneration. The *mdx* muscle in the range of 2–12 mo shows a mild dystrophy relative to human DMD muscle. Our model suggests that the widespread necrotic phase (2–3 wk) leads to well-synchronized regeneration; the severity of the initial necrotic phase may be beneficial in that it may avoid the poorly

Published October 13, 2014

synchronized regeneration and pathology-associated signaling cross talk that occurs in human DMD muscle.

The regenerative asynchrony model may be applicable to chronic pathologies in nonmuscle tissues. Asthma involves chronic inflammation of the airway, where pulsed glucocorticoids are standard of care. In other studies, we have shown that normal epithelial wound repair is synchronous, that remodeling of asthmatic cells is asynchronous and proinflammatory, and that pulsed glucocorticoids restores regenerative synchrony and the nonproinflammatory state (Freishtat et al., 2011; Alcala et al., 2014). One could extend these models to chronic liver pathology, poor skin wound healing, or possibly all chronic inflammatory tissue states leading to fibrosis.

Materials and methods

Human patient muscle samples and mRNA profiles

Flash-frozen neuromuscular disease patient muscle biopsies were taken for diagnostic purposes. Normal control biopsies were obtained from baseline samples from exercise experiments in young adult volunteers.

Two datasets were analyzed. The first (test set) has been previously published (Bakay et al., 2006). This set contained Affymetrix mRNA profiles from 117 patient muscle biopsies using both HG-U133A and HG-U133B microarrays (n = 234 microarrays total; GEO accession no. GSE3307). The muscle disease groups were DMD (n = 10), amyotrophic lateral sclerosis (ALS; n = 9), acute quadriplegic myopathy (n = 5), BMD (n = 5), CAL (calpain III gene mutations; LGMD2A; n = 10), DYSF (LGMD2B; n = 10), ED-R (Emery–Dreifuss muscular dystrophy X linked; n = 4), ED-D (n = 4), FKRP (LGMD2I; n = 7), facioscapulohumeral dystrophy (FSH; n = 14), JDM (n = 21), and normal human skeletal muscle (NHM; n = 18). Biopsies were taken generally at the time of diagnosis and were typically from the vastus lateralis. The original published dataset analyzed 13 groups, but we removed the hereditary spastic paraplegia group from analyses reported here because of a high proportion of outlier transcripts and also removed four JDM samples that were not made public. To generate the mRNA profiles, frozen muscle biopsies were solubilized, total RNA was isolated, RNA was converted into biotinylated cRNA probes, hybridized to Affymetrix microarrays, and detected using fluorescent streptavidin, and microarrays were scanned. Quality control metrics used were as previously reported (Tumor Analysis Best Practices Working Group, 2004).

A second set of 49 human patient mRNA profiles was generated using HG-U133 Plus 2.0 microarrays, and this dataset is new to this study. These datasets contained profiles from 6 normal controls, 17 DMD (absence of dystrophin), 11 BMD (present but abnormal dystrophin), 7 LGMD2I (FKRP deficiency, a glycosylation defect), and 8 LGMD2B (DYSF). Patients had a broad range of ages, clinical severity of their disease, and histopathological findings, although all neuromuscular disease patients showed evidence of a dystrophic process (degeneration/regeneration of muscle fibers). Hematoxylin and eosin stains were performed on frozen sections, and the amount of fibrotic replacement (fibrosis) visually approximated for by the same evaluator (E.P. Hoffman) into normal, mild, moderate, or severe fibrosis categories.

Murine muscle regeneration time series

Staged degeneration/regeneration of adult WT mice was induced by intramuscular injection of cardiotoxin into the entire gastrocnemius muscle using a 10-needle manifold (Zhao and Hoffman, 2004). Mice were sacrificed at 27 time points after the injection, and muscles showing homogenous regeneration were selected for mRNA profiling (n = 2 per time point). Frozen muscle samples were solubilized, total RNA was isolated, RNA was converted to biotinylated cRNA, cRNAs were hybridized to MG-U74Av2 microarrays, and fluorescent images were scanned (GEO accession no. GSE469). Analyses and validations of this degeneration/regeneration time series have been previously published (Zhao et al., 2003, 2006; Zhao and Hoffman, 2004).

Biostatistical clustering methods

We developed a novel method of defining gene clusters within a large multigroup dataset, using the 12-group human muscle biopsy dataset (Fig. S1). Mapped image files from microarrays are interpreted using probe set algorithms that provide probe set normalization, chip normalization, and project normalization so that quantitative signals can be assigned to each probe set (transcript) represented on the microarray. We and others have shown that different probe set algorithms often lead to very different interpretations of the same microarray image files (Seo et al., 2004, 2006; Seo and Hoffman, 2006). To avoid loss of sensitivity for gene selection by using a single probe set algorithm, we simultaneously interpreted the muscle biopsy data using three distinct probe set algorithms (dCHIP, MAS 5.0, and PLIER; Fig. S1). Both A and B microarrays were used, leading to two images with distinct probe sets representing each sample.

Two-way clustering on the rows (genes) and columns (muscular disorders) of the data matrix was performed using the VISDA (Visual Statistical Data Analyzer) software to cluster genes (Fig. S1; Wang et al., 2000, 2007; Zhu et al., 2008). Within each gene cluster, the clustering of the muscular disorders was performed using hierarchical clustering with correlation as the similarity measure after a preprocessing step in which all samples within one muscle group were taken as an average.

This led to a series of probe set algorithm-specific gene clusters that grouped the muscular dystrophies into larger groups based upon the specific microarray used (U133A chip or U133B chip). Thus, PA cluster i refers to PLIER algorithm U133A chip dataset, MA cluster i refers to MAS 5.0 algorithm U133A chip dataset, and dA cluster i refers to dCHIP algorithm U133A chip dataset (Fig. S1 and formulas in this section). Each gene cluster was then tested for gene–gene and gene–protein interactions between cluster members using IPA. The top-ranked networks were then retained for each cluster i (PA network i, MA network i, and dA network i; Fig. S1). We then merged networks and assigned cumulative scores. To accomplish this, we implemented programs to query overlaps among networks and then derived a total score for each network based on its overlaps with all other networks of each gene-disorder pattern. The probability for two networks, S_1 and S_2 with n_1 and n_2 genes, respectively, having m overlapped genes can be calculated as

$$p(m) = \frac{C_N^m C_{N-m}^{n_1-m} C_{N-m}^{n_2-m}}{C_N^{n_1} C_N^{n_2}}, \text{ with}$$

$$\sum_{m=0}^{\min(n_1,n_2)} p(m) = 1,$$

given that S_1, S_2, and the overlapped genes belong to the global network with N genes (N = 26,400, the total number of mammalian genes in Ingenuity Pathway Knowledge base), and C represents a mathematical operation of combination. C of N and m gives the number of subsets of m distinct elements of a set of N elements. Because this probability indicates the likelihood of the overlap of the two networks occurring randomly, $-\log_{10}(p(m))$ may be used as a score for specifying the reliability of the overlap. In addition, the IPA dynamically computes relevant networks by focusing on the genes of interest and delivers a set of scored networks for each gene cluster. A composite score for each network was then calculated by summing up the IPA score and the total score based on network overlaps; the networks were ranked based on their composite scores.

Cross-species query of time series data

Once a gene cluster of interest was selected, probe sets were tested for recognition of canonical transcripts (e.g., 3′ end of well-documented transcript units), and then, these human transcript units were mapped to corresponding rat and mouse transcript units using Affymetrix NetAffx Analysis Center. The Affymetrix probe set IDs corresponding to the transcript units were then queried against the mouse time series data. All mouse image files were analyzed using the PLIER probe set algorithm. Candidate gene clusters were visualized in mouse datasets using heat maps (hierarchical clustering).

All differentially regulated transcripts visualized were tested for statistical significance using t test, without correction for multiple testing. For time series data, adjacent time points were grouped and statistically compared with a relevant control region of the time series.

Asynchronous regeneration protocol

WT BL57 mice of 4–8 wk of age were used for all asynchronous remodeling experiments. To induce asynchronous bouts of regeneration, a 20-guage needle was filled with 10 µl of 5-µg/ml notexin and then dipped in tattoo dye (blue for first injection; red for second injection). Both gastrocnemii were

Published October 13, 2014

surgically exposed, and the initial injection was made distally to proximally along the axis of the muscle. The wound was closed for the number of days indicated, and then, the second injection was performed after the time annotated in each experiment. The initial injection site could be visualized in the muscle as a result of the tattoo dye, and the second injection was initiated adjacent the first site. Mice were euthanized 13 d after the second injury, and gastrocnemii were collected.

For drug treatments with 5 mg/kg/d prednisolone, 15 mg/kg/d VBP15, or vehicle, the drug was delivered in sugar syrup orally. We had five mice in each group. Drug treatments were started 24 h before the initial notexin injection and then continued daily until sacrifice.

Van Gieson measures of fibrotic tissue

Reinjured muscle sections were stained by the Van Gieson method (n = 4 muscles per group). Images were taken and analyzed with ImageJ (National Institutes of Health) to measure the extent of the connective tissue. We assayed the amount of connective tissue per field of tissue by measuring the number of pixels occupied by red staining and then measuring the number of pixels covered by the muscle tissue. The data are then represented as the percentage of muscle that is collagenous connective tissue.

Laser capture microdissection

Flash-frozen muscle biopsies or specimens were sectioned at 10-µm thickness on RNase-free glass slides (CellCut; Molecular Machines & Industries, Inc.). Slides were immediately placed in 99% ethanol to fix. Rapid hematoxylin and eosin stain using RNase-free solutions (Molecular Machines & Industries, Inc.) was then performed followed by laser capture microdissection (CellCut Plus instrument) to identify and cut the areas of interest. We used tubes with an adhesive cap to collect LCM-isolated regions (Molecular Machines & Industries, Inc.).

In brief, 15 consecutive sections for mice at 4 and 10 d were subjected to LCM to isolate each region on each muscle, and cRNA amplification was performed from the combined sections. 3–4 of the 15 LCM sections (per area per mouse) were successful in mRNA profiling, and these showed excellent chip-based clustering. Although the LCM was performed on only one mouse for 4 d and one mouse for 10 d (in part because of the need to identify closely spaced tattoo dye injection sites), additional mice were used for immunostaining validations.

LCM mRNA profiling

RNA isolation was performed using PicoPure kit (Applied Biosystems), which includes on-column DNase digestion. Two rounds of T7-mediated cRNA amplification were performed (RiboAmp HS kit [Applied Biosystems] and then TotalPrep-96 RNA Amplification kit [Life Technologies]). The mRNA profiling on asynchronous mouse LCM experiments was performed in triplicate on serial sections. Murine WG-6 v2.0 Expression BeadChips (Illumina) containing 45,200 transcript probes or HumanHT-12 v4 Expression BeadChips (Illumina) containing 47,000 transcript probes were used. Results of expression arrays were read using the HiScan SQ System (Illumina). Statistical analyses ($P \leq 0.05$ with correction for multiple testing [False Discovery Rate]) and a fold change ≤ 1.5 or ≥ 1.5) were performed to identify dysregulated genes in the areas of interest using Partek Genomics Suite software (Partek, Inc.). IPA was used to query protein–protein and gene–protein interactions.

TaqMan gene expression assay

The RiboAmp HS kit was used to perform two rounds of amplification on total RNA isolated from LCM samples (n = 3 muscles per group) and convert amplified RNA to cDNA. Quantitative gene expression analysis was performed by TaqMan-based qRT-PCR on a real-time PCR system (7900 HT Fast; Applied Biosystems). We used TaqMan Gene Expression kits obtained from Applied Biosystems to run qRT-PCR: Cox6b1 (Mm00824357_m1), Ndufs6 (Mm02529639_u1), Ndufb5 (Mm00452592_m1), Ndufb6 (Mm01208591_g1), and HPRT (hypoxanthine guanine phosphoribosyltransferase; Mm01318747_g1). The expression of HPRT was analyzed as endogenous control simultaneously, and the target gene expression in each sample normalized to HPRT. Thermal cycling conditions were 95°C for 10 min, 50 cycles at 95°C for 15 s, and 60°C for 1 min.

Immunostaining

Monoclonal rat anti–mouse CD11b (eBioscience), mouse anti–human CD74 (Abcam), mouse anti–human macrophage surface antigen (AM-3K/CD163), mouse anti–human mannose receptor (CD206; Abcam), and mouse anti–human MMP9 (Santa Cruz Biotechnology, Inc.) monoclonal primary antibodies were used to perform immunofluorescence assays. The Mouse on Mouse kit (Vector Laboratories) was used to reduce background staining when using mouse monoclonal antibodies on mouse tissue sections (n = 3 muscles per group). Goat anti–mouse (Invitrogen) and goat anti–rat (Invitrogen) secondary antibodies conjugated with Cy3 or Alexa Fluor 488 were used. Nuclei were stained with DAPI (OCHEM). The images were acquired using a fluorescence microscope (BX61; Olympus).

Histochemistry

NADH, SDH, COX, costaining of NADH and COX, Masson's trichrome, and Gomori's modified trichrome were performed on 10-µm biopsy frozen sections to evaluate histology and mitochondrial enzymatic activities (Dubowitz and Sewry, 2007). Murine gastrocnemius 10-µm sections (n = 3 muscles per group) were stained following a standard Van Gieson protocol (Dubowitz and Sewry, 2007). A minimum of nine nonoverlapping images were analyzed in ImageJ for the percentage of connective tissue per field of muscle tissue.

Drug treatment of *mdx* and WT asynchronous remodeling mice

Drug-treated *mdx* mice were from the previously reported preclinical trial comparing 4 mo of 5 mg/kg/d prednisone treatment to 15 mg/kg/d VBP15 treatment (Heier et al., 2013). Frozen archival muscle samples were obtained for WT, *mdx* untreated, and the two drug-treated groups (prednisone and VBP15). RNA was isolated, and mRNA profiling was performed using Illumina bead arrays, according to the manufacturer's protocol (n = 5 per group). Bioinformatics analyses were performed using TGF-β pathway candidates. Drug treatment of the WT asynchronous remodeling mice (n = 5 per group) was performed using the same drugs and treatment regimens (5 mg/kg/d prednisone; 15 mg/kg/d VBP15), with treatment starting the day before the first surgery until the day before euthanasia.

Microscopic image acquisition

All images were acquired using a microscope (BX61; Olympus), with U Plan S Apochromat 20×/0.75 NA dry objective, at room temperature. Photography was performed using a camera (DP11; Olympus) with DP controller 3.2.1.276 and DP Manager 3.1.1.208 software.

Online supplemental material

Fig. S1 shows a flow chart of the data integration and biochemical network analysis on the 12-group human muscle transcriptional profiling data. Fig. S2 shows LCM methods and chip clustering of mRNA profiles of LCM regions of multiply injured muscle. Fig. S3 shows quantitative analysis of endomysial fibrosis in asynchronous remodeled muscle samples. Fig. S4 shows histochemical stains for mitochondrial activity showing a relative loss of mitochondrial oxidative phosphorylation in the area between injuries spaced 4 d apart. Fig. S5 shows treatment of asynchronous remodeling mouse muscle with prednisone or VBP15 suppresses the proinflammatory proteins in between injuries spaced by 4 d. Online supplemental material is available at http://www.jcb.org/cgi/content/full/jcb.201402079/DC1.

This work was supported by the US Department of Defense (W81XWH-05-0334), National Institutes of Health (R01 NS029525, U54 HD053177, and R24 HD050846), Children's National Medical Center Board of Visitors, and the Muscular Dystrophy Association USA. The development of VBP15 is supported by the Congressionally Directed Medical Research Programs of the Department of Defense, Muscular Dystrophy Association Venture Philanthropy program, and the National Institutes of Health National Center for Advancing Translational Sciences, Therapeutics for Rare and Neglected Diseases program.

Competing financial interests: E.P. Hoffman and K. Nagaraju are coinventors of patent WO 2011127048 A3 (Non-hormonal steroid modulators of NF-κB for treatment of disease), and this has been assigned to ReveraGen Biopharma. E.P. Hoffman and K. Nagaraju own founder shares of ReveraGen Biopharma and are members of the Board of Directors. The authors declare no further competing financial interests.

Author contributions: S. Dadgar contributed to the experimental design, data generation and interpretation, and manuscript writing. Z. Wang contributed to the bioinformatics methods development and conduct, figures, and manuscript writing. H. Johnston-Carey contributed to the experimental design, data generation, and writing. A. Kesari contributed to the human muscle biopsy expression profiling design and conduct. K. Nagaraju contributed to the experimental design and data interpretation. Y.-W. Chen contributed to the human muscle biopsy expression profiling design, conduct, and data interpretation. D.A. Hill contributed to the immunohistochemical and histological stains and data interpretation. T. Partridge contributed to the experimental design and data interpretation. M. Giri contributed to the bioinformatics methods and data interpretation. J. Nazarian contributed to the experimental design and data interpretation.

R. Freishtat to the contributed to the experimental design and data interpretation. J. Xuan contributed to the bioinformatics methods development. Y. Wang contributed to the bioinformatics methods development. E.P. Hoffman contributed to the experimental design and interpretation and manuscript writing.

Submitted: 17 February 2014
Accepted: 29 August 2014

References

Aguennouz, M., G.L. Vita, S. Messina, A. Cama, N. Lanzano, A. Ciranni, C. Rodolico, R.M. Di Giorgio, and G. Vita. 2011. Telomere shortening is associated to TRF1 and PARP1 overexpression in Duchenne muscular dystrophy. *Neurobiol. Aging*. 32:2190–2197. http://dx.doi.org/10.1016/j.neurobiolaging.2010.01.008

Akhurst, R.J., and A. Hata. 2012. Targeting the TGFβ signalling pathway in disease. *Nat. Rev. Drug Discov.* 11:790–811. http://dx.doi.org/10.1038/nrd3810

Alcala, S.E., A.S. Benton, A.M. Watson, S. Kureshi, E.M. Reeves, J. Damsker, Z. Wang, K. Nagaraju, J. Anderson, A.M. Williams, et al. 2014. Mitotic asynchrony induces transforming growth factor-β1 secretion from airway epithelium. *Am. J. Respir. Cell Mol. Biol.* 51:363–369. http://dx.doi.org/10.1165/rcmb.2013-0396OC

Alexakis, C., T. Partridge, and G. Bou-Gharios. 2007. Implication of the satellite cell in dystrophic muscle fibrosis: a self-perpetuating mechanism of collagen overproduction. *Am. J. Physiol. Cell Physiol.* 293:C661–C669. http://dx.doi.org/10.1152/ajpcell.00061.2007

Bakay, M., Y.W. Chen, R. Borup, P. Zhao, K. Nagaraju, and E.P. Hoffman. 2002. Sources of variability and effect of experimental approach on expression profiling data interpretation. *BMC Bioinformatics*. 3:4. http://dx.doi.org/10.1186/1471-2105-3-4

Bakay, M., Z. Wang, G. Melcon, L. Schiltz, J. Xuan, P. Zhao, V. Sartorelli, J. Seo, E. Pegoraro, C. Angelini, et al. 2006. Nuclear envelope dystrophies show a transcriptional fingerprint suggesting disruption of Rb-MyoD pathways in muscle regeneration. *Brain*. 129:996–1013. http://dx.doi.org/10.1093/brain/awl023

Baron, D., A. Magot, G. Ramstein, M. Steenman, G. Fayet, C. Chevalier, P. Jourdon, R. Houlgatte, F. Savagner, and Y. Pereon. 2011. Immune response and mitochondrial metabolism are commonly deregulated in DMD and aging skeletal muscle. *PLoS ONE*. 6:e26952. http://dx.doi.org/10.1371/journal.pone.0026952

Bello, L., L. Piva, A. Barp, A. Taglia, E. Picillo, G. Vasco, M. Pane, S.C. Previtali, Y. Torrente, E. Gazzerro, et al. 2012. Importance of SPP1 genotype as a covariate in clinical trials in Duchenne muscular dystrophy. *Neurology*. 79:159–162. http://dx.doi.org/10.1212/WNL.0b013e31825f04ea

Bhattacharyya, S., K. Kelley, D.S. Melichian, Z. Tamaki, F. Fang, Y. Su, G. Feng, R.M. Pope, G.R. Budinger, G.M. Mutlu, et al. 2013. Toll-like receptor 4 signaling augments transforming growth factor-β responses: a novel mechanism for maintaining and amplifying fibrosis in scleroderma. *Am. J. Pathol.* 182:192–205. http://dx.doi.org/10.1016/j.ajpath.2012.09.007

Blau, H M., C. Webster, and G.K. Pavlath. 1983. Defective myoblasts identified in Duchenne muscular dystrophy. *Proc. Natl. Acad. Sci. USA*. 80:4856–4860. http://dx.doi.org/10.1073/pnas.80.15.4856

Bowen, T., R.H. Jenkins, and D.J. Fraser. 2013. MicroRNAs, transforming growth factor beta-1, and tissue fibrosis. *J. Pathol.* 229:274–285. http://dx.doi.org/10.1002/path.4119

Bushby, K., R. Finkel, D.J. Birnkrant, L.E. Case, P.R. Clemens, L. Cripe, A. Kaul, K. Kinnett, C. McDonald, S. Pandya, et al.; DMD Care Considerations Working Group. 2010. Diagnosis and management of Duchenne muscular dystrophy, part 1: diagnosis, and pharmacological and psychosocial management. *Lancet Neurol.* 9:77–93. http://dx.doi.org/10.1016/S1474-4422(09)70271-6

Chen, Y.W., K. Nagaraju, M. Bakay, O. McIntyre, R. Rawat, R. Shi, and E.P. Hoffman. 2005. Early onset of inflammation and later involvement of TGFbeta in Duchenne muscular dystrophy. *Neurology*. 65:826–834. http://dx.doi.org/10.1212/01.wnl.0000173836.09176.c4

Chen, Y.W., R. Shi, N. Geraci, S. Shrestha, H. Gordish-Dressman, and L M. Pachman. 2008. Duration of chronic inflammation alters gene expression in muscle from untreated girls with juvenile dermatomyositis. *BMC Immunol.* 9:43. http://dx.doi.org/10.1186/1471-2172-9-43

Cresswell, P. 1994. Assembly, transport, and function of MHC class II molecules. *Annu. Rev. Immunol.* 12:259–293. http://dx.doi.org/10.1146/annurev.iy.12.040194.001355

Dahiya, S., S. Bhatnagar, S.M. Hindi, C. Jiang, P.K. Paul, S. Kuang, and A. Kumar. 2011a. Elevated levels of active matrix metalloproteinase-9 cause hypertrophy in skeletal muscle of normal and dystrophin-deficient mdx mice. *Hum. Mol. Genet.* 20:4345–4359. http://dx.doi.org/10.1093/hmg/ddr362

Dahiya, S., S. Givvimani, S. Bhatnagar, N. Qipshidze, S.C. Tyagi, and A. Kumar. 2011b. Osteopontin-stimulated expression of matrix metalloproteinase-9 causes cardiomyopathy in the mdx model of Duchenne muscular dystrophy. *J. Immunol.* 187:2723–2731. http://dx.doi.org/10.4049/jimmunol.1101342

Decary, S., C.B. Hamida, V. Mouly, J.P. Barbet, F. Hentati, and G.S. Butler-Browne. 2000. Shorter telomeres in dystrophic muscle consistent with extensive regeneration in young children. *Neuromuscul. Disord.* 10:113–120. http://dx.doi.org/10.1016/S0960-8966(99)00093-0

Dubowitz, V., and C.A. Sewry. 2007. Muscle Biopsy: A Practical Approach. Third edition. Saunders Elsevier, China. 626 pp.

Flanigan, K.M., E. Ceco, K.M. Lamar, Y. Kaminoh, D.M. Dunn, J.R. Mendell, W.M. King, A. Pestronk, J.M. Florence, K.D. Mathews, et al. United Dystrophinopathy Project. 2013. LTBP4 genotype predicts age of ambulatory loss in Duchenne muscular dystrophy. *Ann. Neurol.* 73:481–488. http://dx.doi.org/10.1002/ana.23819

Freishtat, R.J., A.M. Watson, A.S. Benton, S.F. Iqbal, D.K. Pillai, M.C. Rose, and E.P. Hoffman. 2011. Asthmatic airway epithelium is intrinsically inflammatory and mitotically dyssynchronous. *Am. J. Respir. Cell Mol. Biol.* 44:863–869. http://dx.doi.org/10.1165/rcmb.2010-0029OC

Gaschen, F.P., E.P. Hoffman, J.R. Gorospe, E.W. Uhl, D.F. Senior, G.H. Cardinet III, and L.K. Pearce. 1992. Dystrophin deficiency causes lethal muscle hypertrophy in cats. *J. Neurol. Sci.* 110:149–159. http://dx.doi.org/10.1016/0022-510X(92)90022-D

Heier, C.R., J.M. Damsker, Q. Yu, B.C. Dillingham, T. Huynh, J.H. Van der Meulen, A. Sali, B.K. Miller, A. Phadke, L. Scheffer, et al. 2013. VBP15, a novel anti-inflammatory and membrane-stabilizer, improves muscular dystrophy without side effects. *EMBO Mol. Med.* 5:1569–1585. http://dx.doi.org/10.1002/emmm.201302621

Hoffman, E.P., R.H. Brown Jr., and L.M. Kunkel. 1987. Dystrophin: the protein product of the Duchenne muscular dystrophy locus. *Cell*. 51:919–928. http://dx.doi.org/10.1016/0092-8674(87)90579-4

Hoffman, E.P., E. Reeves, J. Damsker, K. Nagaraju, J.M. McCall, E.M. Connor, and K. Bushby. 2012. Novel approaches to corticosteroid treatment in Duchenne muscular dystrophy. *Phys. Med. Rehabil. Clin. N. Am.* 23:821–828. http://dx.doi.org/10.1016/j.pmr.2012.08.003

Holderfield, M.T., and C.C. Hughes. 2008. Crosstalk between vascular endothelial growth factor, notch, and transforming growth factor-beta in vascular morphogenesis. *Circ. Res.* 102:637–652. http://dx.doi.org/10.1161/CIRCRESAHA.107.167171

Irizarry, R.A., D. Warren, F. Spencer, I.F. Kim, S. Biswal, B.C. Frank, E. Gabrielson, J.G. Garcia, J. Geoghegan, G. Germino, et al. 2005. Multiple-laboratory comparison of microarray platforms. *Nat. Methods*. 2:345–350. http://dx.doi.org/10.1038/nmeth756

Karkampouna, S., P. Ten Dijke, S. Dooley, and M.K. Julio. 2012. TGFβ signaling in liver regeneration. *Curr. Pharm. Des.* 18:4103–4113. http://dx.doi.org/10.2174/138161212802430521

Klymiuk, N., A. Blutke, A. Graf, S. Krause, K. Burkhardt, A. Wuensch, S. Krebs, B. Kessler, V. Zakhartchenko, M. Kurome, et al. 2013. Dystrophin-deficient pigs provide new insights into the hierarchy of physiological derangements of dystrophic muscle. *Hum. Mol. Genet.* 22:4368–4382. http://dx.doi.org/10.1093/hmg/ddt287

Koh, M.Y., and G. Powis. 2012. Passing the baton: the HIF switch. *Trends Biochem. Sci.* 37:364–372. http://dx.doi.org/10.1016/j.tibs.2012.06.004

Kollias, H.D., and J.C. McDermott. 2008. Transforming growth factor-beta and myostatin signaling in skeletal muscle. *J. Appl. Physiol.* 104:579–587. http://dx.doi.org/10.1152/japplphysiol.01091.2007

Kornegay, J.N., J.R. Bogan, D.J. Bogan, M.K. Childers, J. Li, P. Nghiem, D.A. Detwiler, C.A. Larsen, R.W. Grange, R.K. Bhavaraju-Sanka, et al. 2012a. Canine models of Duchenne muscular dystrophy and their use in therapeutic strategies. *Mamm. Genome*. 23:85–108. http://dx.doi.org/10.1007/s00335-011-9382-y

Kornegay, J N., M.K. Childers, D.J. Bogan, J.R. Bogan, P. Nghiem, J. Wang, Z. Fan, J.F. Howard Jr., S.J. Schatzberg, J.L. Dow, et al. 2012b. The paradox of muscle hypertrophy in muscular dystrophy. *Phys. Med. Rehabil. Clin. N. Am.* 23:149–172. http://dx.doi.org/10.1016/j.pmr.2011.11.014

Kottlors, M., and J. Kirschner. 2010. Elevated satellite cell number in Duchenne muscular dystrophy. *Cell Tissue Res.* 340:541–548. http://dx.doi.org/10.1007/s00441-010-0976-6

MacDonald, E.M., and R.D. Cohn. 2012. TGFβ signaling: its role in fibrosis formation and myopathies. *Curr. Opin. Rheumatol.* 24:628–634. http://dx.doi.org/10.1097/BOR.0b013e328358df34

Madsen, M., J.H. Graversen, and S.K. Moestrup. 2001. Haptoglobin and CD163: captor and receptor gating hemoglobin to macrophage lysosomes. *Redox Rep.* 6:386–388. http://dx.doi.org/10.1179/135100001101536490

Maier, F., and A. Bornemann. 1999. Comparison of the muscle fiber diameter and satellite cell frequency in human muscle biopsies. *Muscle Nerve*. 22:

578–583. http://dx.doi.org/10.1002/(SICI)1097-4598(199905)22:5<578::AID-MUS5>3.0.CO;2-T

Miyazaki, D., A. Nakamura, K. Fukushima, K. Yoshida, S. Takeda, and S. Ikeda. 2011. Matrix metalloproteinase-2 ablation in dystrophin-deficient mdx muscles reduces angiogenesis resulting in impaired growth of regenerated muscle fibers. *Hum. Mol. Genet.* 20:1787–1799. http://dx.doi.org/10.1093/hmg/ddr062

Nghiem, P.P., E.P. Hoffman, P. Mittal, K.J. Brown, S.J. Schatzberg, S. Ghimbovschi, Z. Wang, and J.N. Kornegay. 2013. Sparing of the dystrophin-deficient cranial sartorius muscle is associated with classical and novel hypertrophy pathways in GRMD dogs. *Am. J. Pathol.* 183:1411–1424. http://dx.doi.org/10.1016/j.ajpath.2013.07.013

Niimi, H., K. Pardali, M. Vanlandewijck, C.H. Heldin, and A. Moustakas. 2007. Notch signaling is necessary for epithelial growth arrest by TGF-β. *J. Cell Biol.* 176:695–707. http://dx.doi.org/10.1083/jcb.200612129

Oexle, K., A. Zwirner, K. Freudenberg, A. Kohlschütter, and A. Speer. 1997. Examination of telomere lengths in muscle tissue casts doubt on replicative aging as cause of progression in Duchenne muscular dystrophy. *Pediatr. Res.* 42:226–231. http://dx.doi.org/10.1203/00006450-199708000-00016

Pegoraro, E., E.P. Hoffman, L. Piva, B.F. Gavassini, S. Cagnin, M. Ermani, L. Bello, G. Soraru, B. Pacchioni, M.D. Bonifati, et al.; Cooperative International Neuromuscular Research Group. 2011. SPP1 genotype is a determinant of disease severity in Duchenne muscular dystrophy. *Neurology*. 76:219–226. http://dx.doi.org/10.1212/WNL.0b013e318207afeb

Philippou, A., M. Maridaki, and M. Koutsilieris. 2008. The role of urokinase-type plasminogen activator (uPA) and transforming growth factor beta 1 (TGFbeta1) in muscle regeneration. *In Vivo*. 22:735–750.

Sali, A., A.D. Guerron, H. Gordish-Dressman, C.F. Spurney, M. Iantorno, E.P. Hoffman, and K. Nagaraju. 2012. Glucocorticoid-treated mice are an inappropriate positive control for long-term preclinical studies in the mdx mouse. *PLoS ONE*. 7:e34204. http://dx.doi.org/10.1371/journal.pone.0034204

Seo, J., and E.P. Hoffman. 2006. Probe set algorithms: is there a rational best bet? *BMC Bioinformatics*. 7:395. http://dx.doi.org/10.1186/1471-2105-7-395

Seo, J., M. Bakay, Y.W. Chen, S. Hilmer, B. Shneiderman, and E.P. Hoffman. 2004. Interactively optimizing signal-to-noise ratios in expression profiling: project-specific algorithm selection and detection p-value weighting in Affymetrix microarrays. *Bioinformatics*. 20:2534–2544. http://dx.doi.org/10.1093/bioinformatics/bth280

Seo, J., H. Gordish-Dressman, and E.P. Hoffman. 2006. An interactive power analysis tool for microarray hypothesis testing and generation. *Bioinformatics*. 22:808–814. http://dx.doi.org/10.1093/bioinformatics/btk052

Serrano, A.L., C.J. Mann, B. Vidal, E. Ardite, E. Perdiguero, and P. Muñoz-Cánoves. 2011. Cellular and molecular mechanisms regulating fibrosis in skeletal muscle repair and disease. *Curr. Top. Dev. Biol.* 96:167–201. http://dx.doi.org/10.1016/B978-0-12-385940-2.00007-3

Solovjov, D.A., E. Pluskota, and E.F. Plow. 2005. Distinct roles for the α and β subunits in the functions of integrin αMβ2. *J. Biol. Chem.* 280:1336–1345. http://dx.doi.org/10.1074/jbc.M406968200

Tezak, Z., E.P. Hoffman, J.L. Lutz, T.O. Fedczyna, D. Stephan, E.G. Bremer, I. Krasnoselska-Riz, A. Kumar, and L.M. Pachman. 2002. Gene expression profiling in DQA1*0501+ children with untreated dermatomyositis: a novel model of pathogenesis. *J. Immunol.* 168:4154–4163. http://dx.doi.org/10.4049/jimmunol.168.8.4154

Tumor Analysis Best Practices Working Group. 2004. Expression profiling—best practices for data generation and interpretation in clinical trials. *Nat. Rev. Genet.* 5:229–237. http://dx.doi.org/10.1038/nrg1297

Villalta, S.A., H.X. Nguyen, B. Deng, T. Gotoh, and J.G. Tidball. 2009. Shifts in macrophage phenotypes and macrophage competition for arginine metabolism affect the severity of muscle pathology in muscular dystrophy. *Hum. Mol. Genet.* 18:482–496. http://dx.doi.org/10.1093/hmg/ddn376

Wang, J., H. Li, Y. Zhu, M. Yousef, M. Nebozhyn, M. Showe, L. Showe, J. Xuan, R. Clarke, and Y. Wang. 2007. VISDA: an open-source caBIG analytical tool for data clustering and beyond. *Bioinformatics*. 23:2024–2027. http://dx.doi.org/10.1093/bioinformatics/btm290

Wang, Y., L. Luo, M.T. Freedman, and S.Y. Kung. 2000. Probabilistic principal component subspaces: a hierarchical finite mixture model for data visualization. *IEEE Trans. Neural Netw.* 11:625–636. http://dx.doi.org/10.1109/72.846734

Watkins, S.C., and M.J. Cullen. 1986. A quantitative comparison of satellite cell ultrastructure in Duchenne muscular dystrophy, polymyositis, and normal controls. *Muscle Nerve*. 9:724–730. http://dx.doi.org/10.1002/mus.880090808

Watkins, S.C., and M.J. Cullen. 1988. A quantitative study of myonuclear and satellite cell nuclear size in Duchenne's muscular dystrophy, polymyositis and normal human skeletal muscle. *Anat. Rec.* 222:6–11. http://dx.doi.org/10.1002/ar.1092220103

Zhao, P., and E.P. Hoffman. 2004. Embryonic myogenesis pathways in muscle regeneration. *Dev. Dyn.* 229:380–392. http://dx.doi.org/10.1002/dvdy.10457

Zhao, P., J. Seo, Z. Wang, Y. Wang, B. Shneiderman, and E.P. Hoffman. 2003. In vivo filtering of in vitro expression data reveals MyoD targets. *C. R. Biol.* 326:1049–1065. http://dx.doi.org/10.1016/j.crvi.2003.09.035

Zhao, P., G. Caretti, S. Mitchell, W.L. McKeehan, A.L. Boskey, L.M. Pachman, V. Sartorelli, and E.P. Hoffman. 2006. Fgfr4 is required for effective muscle regeneration in vivo. Delineation of a MyoD-Tead2-Fgfr4 transcriptional pathway. *J. Biol. Chem.* 281:429–438. http://dx.doi.org/10.1074/jbc.M507440200

Zhu, Y., H. Li, D.J. Miller, Z. Wang, J. Xuan, R. Clarke, E.P. Hoffman, and Y. Wang. 2008. caBIG VISDA: modeling, visualization, and discovery for cluster analysis of genomic data. *BMC Bioinformatics*. 9:383. http://dx.doi.org/10.1186/1471-2105-9-383

Natural Progression of Childhood Asthma Symptoms and Strong Influence of Sex and Puberty

Liang Fu[1], Robert J. Freishtat[2,3,4], Heather Gordish-Dressman[2,4], Stephen J. Teach[3], Lorenzo Resca[1,5], Eric P. Hoffman[2,4], and Zuyi Wang[1,2,4]

[1]Division of Research and Development, SoverST, LLC, Rockville, Maryland; [2]Department of Integrative Systems Biology, George Washington University School of Medicine and Health Sciences, Washington, DC; [3]Division of Emergency Medicine, and [4]Research Center for Genetic Medicine, Children's National Health System, Washington, DC; and [5]Department of Physics, The Catholic University of America, Washington, DC

Abstract

Rationale: Asthma prevalence, onset, remission and relapse, and healthcare use have been intensively studied. However, asthma symptom progression through childhood and adolescence has not been well studied, in part due to the challenges in obtaining consistent and robust long term follow up data on a large series of subjects with asthma.

Objectives: To use the asthma diary symptom data of the Childhood Asthma Management Program placebo group (5 yr, 418 subjects, and total 564,518 records) to establish sex specific high resolution time courses of the natural progression of asthma symptoms through childhood and adolescence.

Methods: We used the asthma diary symptom code as a measure of daily disease severity. Annual records of Tanner stage were used to determine the influence of puberty on severity. A data alignment technique was used to derive 13 year time courses of mean symptoms and mean Tanner stage.

Measurements and Main Results: Data analyses showed three age and sex related phases of asthma symptom progression: Phase 1 (ages 5 and 6 yr) greater severity in boys; Phase 2 (ages 7 to 9 yr) no sex difference in severity; and Phase 3 (age 10 17 yr) greater severity in girls. The continuous decline of symptoms in both sexes stops abruptly at the onset of puberty.

Conclusions: The severity of asthma symptoms varies through childhood and adolescence, and patterns differ by sex. Puberty has a strong influence on symptom progression in both sexes. Progression of symptoms is a distinct aspect of asthma epidemiology.

Keywords: epidemiology; sex difference; sex dominance

(Received in original form February 27, 2014; accepted in final form May 26, 2014)

Supported by Clark Charitable Foundation (E.P.H. and R.J.F.) and National Institutes of Health grant R01MD007075 (R.J.F.).

Author Contributions: L.F., R.J.F., H.G. D., L.R., and Z.W. were responsible for study design, data analyses, and interpretation. S.J.T. and E.P.H. contributed to drafting and revising the article.

Correspondence and requests for reprints should be addressed to Zuyi Wang, Ph.D., Center for Genetic Medicine, Children's National Health System, 111 Michigan Ave, NW, Washington, DC 20010. E mail: zwang@childrensnational.org.

This article has an online supplement, which is accessible from this issue's table of contents at www.atsjournals.org

Ann Am Thorac Soc Vol 11, No 6, pp 939 944, Jul 2014

DOI: 10.1513/AnnalsATS.201402 084OC
Internet address: www.atsjournals.org

The progression of asthma symptoms through childhood and adolescence is complex, variable, and poorly understood. Asthma is known to affect males more in childhood and females more in adulthood (1 3). Studies supporting this observation have focused on four epidemiologic aspects of the disease: (*1*) cross sectional prevalence (4 17), (*2*) onset (18 20), (*3*) remission and relapse (21 31), and (*4*) healthcare use (32 40).

Study on each of the four aspects requires unique type of data and only provides a partial view of asthma epidemiology. Prevalence studies of asthma collect data from a general population and describe the percentage of participants with asthma. Studies of asthma onset follow a population without asthma and describe a one way Boolean (yes or no) transition of developing asthma. Studies of asthma remission and relapse follow a population with asthma and describe a two way Boolean transition. Studies of asthma healthcare use describe a mixed effect of prevalence and symptom severity (both higher prevalence and more severe symptoms tend to contribute more).

There is another important aspect of asthma epidemiology, namely, the progression of asthma symptoms. Differing

from the above four aspects, studying asthma symptom progression generally has to follow a population with asthma and quantitatively describes the temporal change of symptom severity. The existing studies on prevalence, onset, remission and relapse, and healthcare use do not directly describe the longitudinal progression of asthma symptoms.

Presently, there is little knowledge on how symptoms vary with age and between two sexes. Herein, we attempt to fill this knowledge gap by analyzing the data of the Childhood Asthma Management Program (CAMP) (41). We expect that sex and age significantly affect the symptom progression, just like they affect the other four aspects of asthma epidemiology. However, we expect that the trend and properties of symptom progression will differ from those of the other four aspects. In addition, we investigate whether puberty influences the symptom progression.

Methods

The CAMP and its continuation study are the largest and longest clinical studies in children with mild to moderate asthma. The objective of CAMP is to study the long term effect of regular use of asthma control medication on the growth of children with asthma. To study the progression of symptoms unaffected by any intervention, we analyzed the CAMP asthma symptom code variable (XSYMP) of diary data from the CAMP placebo group: 5 years of daily records of symptom data from 418 participants (184 girls, 234 boys), total 564,518 records. To define the influence of puberty on symptom progression in each sex, we also analyzed the Tanner stage data of the CAMP placebo group.

CAMP Diary Symptom Data

The symptom code, XSYMP, of the CAMP diary data of the placebo group was used to study the natural progression of asthma symptoms from childhood through adolescence. The XSYMP code is defined as follows:

An asthma episode is a single period of one or more asthma "stop signs," such as wheezing, coughing, chest tightness, or shortness of breath;

- 0 = no asthma episodes;
- 1 = one to three asthma episodes, each lasting 2 hours or less, all mild;
- 2 = four or more mild asthma episodes, or one or more asthma episodes that temporarily interfered with activity, play, school, or sleep;
- 3 = one or more asthma episodes lasting longer than 2 hours, or resulting in shortening normal activity, or seeing a doctor for acute care, or going to a hospital for acute care.

The CAMP XSYMP data provide an objective, quantitative, and daily measure of the severity of asthma symptoms.

CAMP Tanner Stage Data

The pubic hair data of the placebo group were used to study the influence of puberty on asthma symptom progression.

All the CAMP data used in this study were obtained from BioLINCC (https://biolincc.nhlbi.nih.gov/home, Biologic Specimen and Data Repository Information Coordinating Center). Additional information about the CAMP diary symptom data code is available on the website of CAMP on www.ClinicalTrials.gov. The protocol of this study has been approved by the Institutional Review Board (Pro00002700).

Aligning Samples by Age

The CAMP participants can be divided into eight age groups according to their ages at enrollment (age 5, 6, 7, 8, 9, 10, 11, and 12 yr at enrollment); the XSYMP and Tanner stage data of each age group span approximately 5 years. We used Aligning Samples by Age to generate sex specific 13 year long time courses of mean XSYMP and mean Tanner stage for the CAMP placebo group. The procedure of Aligning Samples by Age is as follows: (*1*) the date when each measurement was taken is converted to a subject's age (age X denotes the range [X 0.5 yr, X+0.5 yr]), (*2*) the measurements that fall into the same age are grouped. This method allows us to fully use the CAMP data to generate long coverage time courses.

Modeling the Distribution of XSYMP

A truncated Poisson distribution, $T(X=k)=\frac{\lambda^k/k!}{\sum_{l=0}^{3}\lambda^l/l!}$ $(k=0,1,2,3)$, was used to model the distribution of XSYMP of each time point for each sex. k was truncated after 3 because the diary symptom code has only four values: 0, 1, 2, and 3. The actual histogram of XSYMP of each time point was compared with the fitted truncated Poisson distribution, and χ^2 was calculated to assess the goodness of fit.

We found that the distribution of XSYMP of each time point and for each sex can be accurately modeled by the truncated Poisson distribution (Figure 1; details in RESULTS). The average χ^2 (over all of the

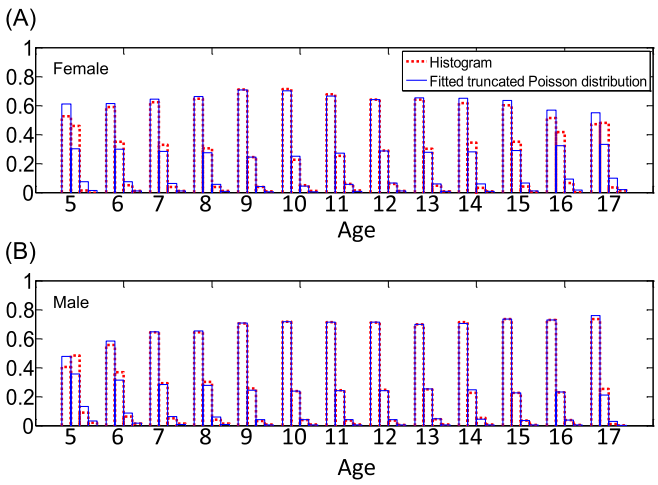

Figure 1. Modeling of the diary symptom code data, XSYMP (Childhood Asthma Management Program [CAMP] placebo group), by truncated Poisson distribution. The truncated Poisson distribution (*blue*) was fitted to the actual histogram (*red*) of XSYMP at each time point for girls (*A*) and boys (*B*). As an evaluation of the goodness of fit, the average χ^2 (over all time points) is 0.01 for girls and 0.004 for boys. The results demonstrated that the XSYMP data of all time points in both sex specific time courses can be accurately modeled by the truncated Poisson distribution. The four bins (from *left* to *right*) in each histogram correspond to the four values of XSYMP: 0, 1, 2, and 3; the details about XSYMP are in METHODS and the online supplement.

4C/FPO

included time points) as a measure of fitting error was 0.01 for girls and 0.004 for boys. These results set the foundation of our data analysis, and specifically set the following important grounds (details in RESULTS):

1. Statistically, the XSYMP samples of each time point for each sex can be treated as independent samples drawn from the specific truncated Poisson distribution;
2. The distribution of XSYMP can be summarized by a single parameter;
3. For our specific truncated Poisson distribution (truncated after $k = 3$ and $\lambda \leqslant 0.75$), 30 samples are sufficient to ensure that the SE and bootstrapping SD equal the true SD of the mean.

According to ground 1, the XSYMP samples are independent from the subject who contributed the samples; therefore, the statistical significance is determined by the number of XSYMP samples rather than the number of subjects. The number of subjects would matter if XSYMP samples naturally cluster by subjects and follow a mixture of distributions (42). However, we have demonstrated that XSYMP samples fit accurately to a truncated Poisson distribution (a single distribution), proving that the XSYMP samples do not cluster by subjects.

Generally speaking, the mean of a variable with ordinal scale (XSYMP is a variable of ordinal scale) may not be meaningful. However, the fact that XSYMP accurately follows truncated Poisson distribution makes mean XSYMP meaningful, as explained below. Truncated Poisson distribution has only one parameter, λ, and λ is monotonically related to the mean (either one can be uniquely determined by the other, and they increase and decrease together). Therefore, mean XSYMP can be used to describe symptoms instead of λ because it completely determines the distribution of XSYMP. As mean XSYMP increases, the mass of XSYMP moves toward larger values (more severe symptoms) or vice versa; hence, mean XSYMP provides a concise and continuous measure for the symptoms.

In addition, ground 3 alone (without arguing the independence of the samples) ensures that SE (hence the 95% confidence interval [CI]) accurately assesses the variance of the mean XSYMP (there are thousands or even tens of thousands XSYMP samples for each time point; Table 1).

Table 1. The numbers of subjects and diary records for each time point in the asthma symptom time courses

Age, yr	Female		Male	
	Subjects	Diary Records	Subjects	Diary Records
5	8	477	16	1,470
6	29	6,429	52	10,407
7	51	11,342	83	22,187
8	76	19,765	114	30,713
9	101	27,956	148	41,690
10	130	32,022	169	45,028
11	141	37,164	166	43,762
12	142	36,303	153	38,181
13	116	28,371	135	36,406
14	86	18,839	102	26,006
15	60	12,067	73	16,561
16	31	4,987	46	9,983
17	11	1,593	28	4,809

Childhood Asthma Management Program placebo group. As established in METHODS, the statistical significance is determined by the number of diary records rather than the number of subjects.

Generating Asthma Symptoms and Tanner Stage Time Courses

We use Aligning Samples by Age to generate sex specific mean XSYMP and mean Tanner stage time courses that cover from age 5 to 17 years. Note that although Tanner stage by definition is discrete (integers from 1 5), the pubertal development is naturally a continuous process. When this continuous process is described by discrete values, rounding errors (presumably follow a uniform distribution from 0.5 to 0.5) are produced. The rounding errors can be largely eliminated by averaging. Therefore, mean Tanner stage actually provides a more accurate description of the pubertal development. Tanner staging of the CAMP participants was performed once a year by the medical staff at the CAMP centers based on a well defined somatic growth measures manual; hence, the data are more accurate than self reported or parent reported Tanner staging data.

Additional details about the data and method are in the online data supplement.

Results

Statistical Results of the Distribution Modeling of XSYMP

We found that the distribution of XSYMP at each time point and for each sex can be accurately modeled by the truncated Poisson distribution (Figure 1). The average χ^2 (over all time points) as a measure of fitting error was 0.01 for girls and 0.004 for boys. Smaller χ^2 was achieved at the time points with larger sample sizes. For example, the fitting for the middle time points (where sample sizes are larger) was better than the end time points (Figure 1). Also, the fitting was generally better for boys than for girls, because the sample sizes are larger for boys for all time points (Table 1). These are strong indications that the truncated Poisson distribution is indeed the appropriate model for the distribution of XSYMP data. Model fitting of such high accuracy is rare in epidemiological studies of asthma, which is attributed to the high quality and high volume of the CAMP diary symptom data.

Using bootstrapping, we estimated the minimum number of samples required to achieve sound statistics in the distribution of XSYMP at each time point. By simulation, we have found that for $\lambda \leqslant 0.75$ (for the distribution of XSYMP), with a minimum of 30 samples, both the SE and bootstrap SD accurately match the true SD of the mean. As the sample size N further increases, all these three quantities remain essentially identical and scale as $1/\sqrt{N}$, precisely as predicted by the central limit theorem. The number of XSYMP samples for each sex at each time point is typically in thousands or even tens of thousands (Table 1). This exceptionally large volume of XSYMP data results in remarkably small statistical uncertainty, which is demonstrated by extremely small 95% CIs for all time

points in the time courses of mean XSYMP (Figure 2A). Similarly high statistical certainty has also been obtained in the time course of mean Tanner stage (Figure 2B).

Additional details about the statistical methods for data distribution modeling are in the online data supplement.

Influences of Sex, Puberty, and Age on Asthma Symptom Progression

Using the high resolution time courses of symptoms and Tanner stage, we distinguish the influences of age and puberty (two concurrent influencing variables) and show that puberty has a strong influence on symptom progression in both sexes. Specifically, the onset of puberty in both sexes is the critical turning point of symptom progression: Symptoms in both sexes stop improving at the onset of puberty; girls' symptoms deteriorate during puberty and boys' symptoms do not improve until late puberty.

The symptom time courses (Figure 2A) show sex differences in progression of asthma symptoms through childhood and adolescence, ages 5 to 17 years, and there are essentially three distinct phases at these ages.

Phase 1 (ages 5 and 6 yr) greater severity in boys. Boys had more severe symptoms than girls before age 7 years, and symptoms in both sexes improved. The mean XSYMP values (95% CI) of boys and girls were 0.72 (0.69 0.76) and 0.49 (0.44 0.54), respectively, at age 5 years, and declined to 0.44 (0.43 0.45) and 0.43 (0.43 0.44), respectively, at age 7 years. The sex difference in symptoms gradually and consistently diminished during this time.

Phase 2 (ages 7 to 9 yr) no difference in severity by sex. The sex difference in symptoms was essentially indistinguishable at ages 7 to 9 years. Additionally, the continuous decline of symptoms stopped around age 9 for girls and age 10 for boys. Based on the Tanner stage time courses (Figure 2B) of the same subjects, ages 9 and 10 years mark the onset of puberty for female and male participants, respectively. Furthermore, the curve of mean XSMYP versus mean Tanner stage (Figure 2C) shows that the continuous decline in symptoms in both sexes stops abruptly when the mean Tanner stage begins to rise from 1 (onset of puberty).

Phase 3 (ages 10 to 17 yr) greater severity in girls. Greater severity of symptoms among girls starts around age 10 years, after the halt of symptom improvement in both girls and boys, and the severities in the two sexes become more far apart along puberty. Between ages 10 and 14 years, girls' symptoms start to worsen, and boys' symptoms remain stable. At late puberty, boys' symptoms resume improvement, and girls' symptoms continue to worsen. At age 17 years, the mean XSYMP value (95% CI) of girls reached 0.59 (0.56 0.62) (worse than their symptoms at age 5 yr), but that of boys dropped to 0.28 (0.26 0.29).

The trend of symptom progression can also be observed, perhaps in more detail, by comparing the distributions of asthma symptom code, XSYMP, of all the time points (Figure 1). For girls (Figure 1A), from ages 5 to 9 years, the mass of the distribution moves from larger symptom

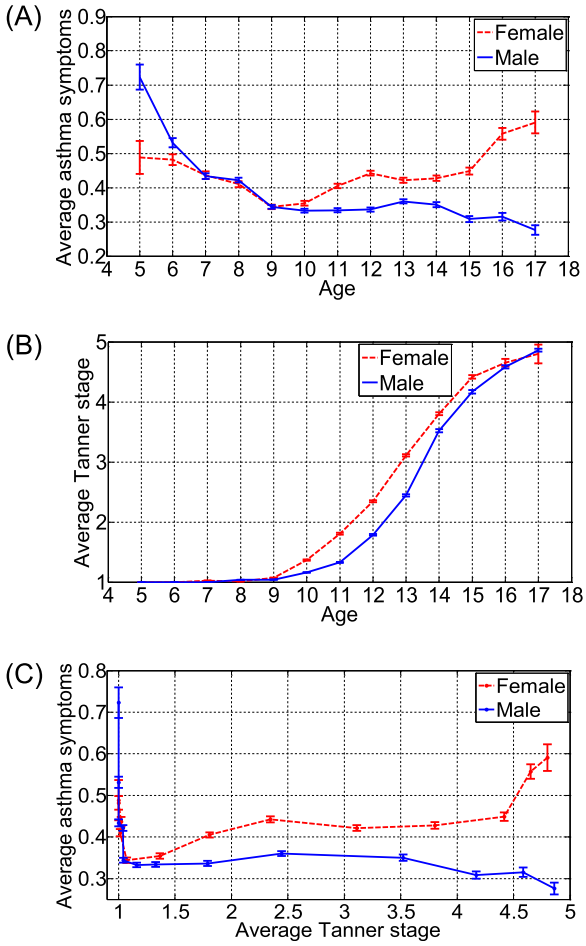

Figure 2. Sex specific time courses of mean XSYMP and mean Tanner stage (Childhood Asthma Management Program [CAMP] placebo group). (*A*) We used Aligning Samples by Age to generate the sex specific time courses of mean Tanner stage. Note that the Tanner stage is discrete number (1 5), but the mean Tanner stage is continuous. The error bars are 95% confidence intervals (CIs) (some are too small to be visible). These curves are highly consistent with the documented puberty development data, demonstrating the effectiveness of this method. (*B*) Using Aligning Samples by Age, we generated the sex specific time courses of mean XSYMP. The time courses have high time resolution (with time interval of 1 year) and long coverage (covering 13 years, ages 5 to 17 years). Note that age X in the time course denotes the range [X−0.5, X+0.5). The extremely small 95% CIs (*error bars*) indicate the high statistical power of CAMP diary symptom data. (*C*) The curve of mean XSYMP versus mean Tanner stage. This curve shows that the continuous decline of symptom severity in both sexes stops abruptly and the female sex dominance in severity starts precisely at the onset of puberty where the mean Tanner stage just departs from the value of 1. This indicates that puberty is a critical stage in symptom progression. With high temporal resolution and parallel Tanner stage data, we are able to clearly distinguish between the influences of two concurrent variables (i.e., age and puberty). The sudden interruptions of continuous symptom improvements at the onset of puberty in both sexes can only be attributed to puberty.

codes (e.g., non zero codes) to smaller symptom codes (e.g., zero code). In other words, the participants gradually had fewer days with asthma episodes or with longer and more episodes from ages 5 to 9 years. After age 9 years, the opposite happened; the mass distribution moves back toward larger symptom codes for girls. For boys (Figure 1B), the mass of the distribution also moves toward smaller symptom codes from ages 5 to 10 years; during age 10 to 14 years, the distribution essentially remains unchanged, and after age 14 years the mass of the distribution again moves toward smaller symptom codes.

Discussion

Our study finds that the properties of asthma symptom progression distinctly differ from those of asthma prevalence. First, despite the large variations, previous studies generally indicate that a higher male prevalence continues at least to age 16 years (some studies even indicate that a higher male prevalence continues well into adulthood) (4, 8, 10, 12, 14, 17, 31). However, our results show that greater severity of symptoms among boys stops at age 7 years. Second, previous studies all show that the asthma sex dominance reversal is a simple crossover. Our results show a more nuanced pattern in symptom progression: symptoms of both sexes go through a short period of similarity, with sex differences disappearing at ages 7, 8, and 9 years before reversing and diverging. Third, puberty was shown to have minimal or no influence on prevalence (43 46). Our results show that puberty has a strong influence on altering the courses of asthma progression in both sexes and that it is associated with the reversal of sex dominance in symptom severity. All above evidences show that symptom progression is a distinct aspect of asthma epidemiology, and its properties cannot be deduced from those of other aspects.

Asthma exacerbations are usually episodic; therefore, asthma symptoms, regardless of how defined and measured, have substantial fluctuations among individuals and within individual over time. To generate reliable symptom time courses, sufficient subjects and frequent measurements of symptoms for each subject at each time point are necessary to ensure satisfactory statistical certainty of symptom severity value at each time point. Besides, symptom data that cover many densely distributed time points are required for generating long coverage and high resolution time courses. Due to these challenges in obtaining such suitable symptom data, symptom progression has never been well defined. The CAMP diary symptom data (XSYMP) provide a rare opportunity in this regard. From the data distribution modeling and statistical analysis of XSYMP, we demonstrated the reliability of the symptom time courses generated in this study. In addition, diary symptom data have important advantages over questionnaire data that are often collected in many asthma cohort studies. First, daily recording of symptoms benefits from fresh memory. In contrast, a questionnaire typically asks the respondent to recall asthma related incidences during a certain period in the past (e.g., past 6 months). If this period is too short, the answers may not accurately reflect symptoms of the respondent, given the episodic nature of asthma. If this period is too long, not only is the temporal resolution reduced but accuracy may be compromised. Second, diary data provide the possibility of building high resolution symptom time courses.

Given the distribution of the participants in the CAMP placebo group over racial categories (around 70% white, 30% black, Hispanic, and others; details in the online supplement), the results and conclusions of this study can be applied to the general population of the United States.

The finding of this study regarding the influence of puberty on asthma symptoms suggests that sex hormones potentially play an important role in the pathogenesis of asthma. Indeed, a body of compelling evidence supports the link between female sex hormones and the development of asthma and exacerbations of asthma during menstruation (47, 48) and potential protective effects of testosterone on asthma due to its immunosuppressing function (49). However, the exact mechanisms are unclear. In addition, our previous study found differential expressions of immune response genes of innate and adaptive immune systems in female and male mice during puberty, suggesting that the sexual dimorphism seen in postpubertal life start forming in puberty (50). Moreover, our study demonstrates that puberty is a critical stage in asthma symptom progression in both sexes. Future studies may focus on this specific period, and the ages immediately before and after, to identify the role of sex hormones on pulmonary physiology, immunology, and pathology of asthma.

In conclusion, we have established sex specific high resolution time courses for the natural progression of asthma symptoms through childhood and adolescence. Together with the parallel Tanner stage time courses, we untangle the effects of two concurrent variables, age and puberty. The sudden interruption of the trend that occurs at the onset of puberty for both sexes strongly suggests a much greater association between asthma symptoms and puberty rather than with age at that stage. The small 95% CIs of the mean symptom code at each time point in these time courses demonstrate statistical reliability of our results. We thus found that puberty had a strong influence on the progression of asthma symptoms in both sexes and was associated with sex reversal in symptom severity. Our results show that asthma symptom progression is a distinct aspect of asthma epidemiology and that its properties substantially differ from those of the other aspects, namely, prevalence, onset, remission and relapse, and healthcare use. ■

Author disclosures are available with the text of this article at www.atsjournals.org.

References

1 Almqvist C, Worm M, Leynaert B; working group of GA2LEN WP 2.5 Gender. Impact of gender on asthma in childhood and adolescence: a GA2LEN review. *Allergy* 2008;63:47 57.
2 Choi IS. Gender specific asthma treatment. *Allergy Asthma Immunol Res* 2011;3:74 80.
3 McCallister J, Mastronarde J. Sex differences in asthma. *J Asthma* 2008;45:853 861.
4 Anderson H, Pottier A, Strachan D. Asthma from birth to age 23: incidence and relation to prior and concurrent atopic disease. *Thorax* 1992;47:537 542.
5 Bjerg Backlund AJ, Perzanowski MS, Platts Mills T, Sandstrom T, Lundback B, Ronmark E. Asthma during the primary school

ages prevalence, remission and the impact of allergic sensitization. *Allergy* 2006;61:549 555.
6 Carlsen KCLHG, Devulapalli CS, Munthe Kaas M, Pettersen M, Granum B, Løvik M, Carlsen KH. Asthma in every fifth child in Oslo, Norway: a 10 year follow up of a birth cohort study. *Allergy* 2006;61: 454 460.
7 Devenny A, Wassall H, Ninan T, Omran M, Khan S, Russell G. Respiratory symptoms and atopy in children in Aberdeen: questionnaire studies of a defined school population repeated over 35 years. *BMJ* 2004;329:489 490.
8 Leynaert BSJ, Garcia Esteban R, Svanes C, Jarvis D, Cerveri I, Dratva J, Gislason T, Heinrich J, Janson C, Kuenzli N, *et al*. Gender differences in prevalence, diagnosis and incidence of allergic and non allergic asthma: a population based cohort. *Thorax* 2012;67: 625 631.
9 Lichtenstein P, Svartengren M. Genes, environments, and sex: factors of importance in atopic diseases in 7 9 year old Swedish twins. *Allergy* 1997;52:1079 1086.
10 Moorman JE, Rudd RA, Johnson CA, King M, Minor P, Bailey C, Scalia MR, Akinbami LJ. National surveillance for asthma United States, 1980 2004. *MMWR Surveill Summ* 2007;56:1 54.
11 Osman M. Therapeutic implications of sex differences in asthma and atopy. *Arch Dis Child* 2003;88:587 590.
12 Strachan D, Butland B, Anderson H. Incidence and prognosis of asthma and wheezing illness from early childhood to age 33 in a national British cohort. *BMJ* 1996;312:1195 1199.
13 Wijga ATC, Postma D, Kerkhof M, Wieringa M, Hoekstra M, Brunekreef B, de Jongste J, Smit H. Sex differences in asthma during the first 8 years of life: the Prevention and Incidence of Asthma and Mite Allergy (PIAMA) birth cohort study. *J Allergy Clin Immunol* 2011;127: 275 277.
14 Wright A, Stern D, Kauffmann F, Martinez F. Factors influencing gender differences in the diagnosis and treatment of asthma in childhood: the Tucson Children's Respiratory Study. *Pediatr Pulmonol* 2006;41: 318 325.
15 PausJenssen ES, Cockcroft DW. Sex differences in asthma, atopy, and airway hyperresponsiveness in a university population. *Ann Allergy Asthma Immunol* 2003;91:34 37.
16 van Merode T, Maas T, Twellaar M, Kester A, van Schayck C. Gender specific differences in the prevention of asthma like symptoms in high risk infants. *Pediatr Allergy Immunol* 2007;18:196 200.
17 Akinbami LJ, Moorman JE, Liu X. Asthma prevalence, health care use, and mortality: United States, 2005 2009. *Natl Health Stat Report* 2011;32:1 16.
18 de Marco RLF, Cerveri I, Bugiani M, Marinoni A, Giammanco G; Italian Study on Asthma in Young Adults study group. Incidence and remission of asthma: a retrospective study on the natural history of asthma in Italy. *J Allergy Clin Immunol* 2002;110:228 235.
19 Mandhane P, Greene J, Cowan J, Taylor D, Sears M. Sex differences in factors associated with childhood and adolescent onset wheeze. *Am J Respir Crit Care Med* 2005;172:45 54.
20 Rudd R, Moorman J. Asthma incidence: data from the National Health Interview Survey, 1980 1996. *J Asthma* 2007;44:65 70.
21 Bronnimann S, Burrows B. A prospective study of the natural history of asthma. Remission and relapse rates. *Chest* 1986;90:480 484.
22 Burgess JMM, Gurrin L, Byrnes G, Adams K, Wharton C, Giles G, Jenkins M, Hopper J, Abramson M, Walters E, *et al*. Factors influencing asthma remission: a longitudinal study from childhood to middle age. *Thorax* 2011;66:508 513.
23 Ekerljung LRE, Larsson K, Sundblad BM, Bjerg A, Ahlstedt S, Dahlén SE, Lundback B. No further increase of incidence of asthma: incidence, remission and relapse of adult asthma in Sweden. *Respir Med* 2008;102:1730 1736.
24 Holm MOE, Gíslason T, Svanes C, Jogi R, Norrman E, Janson C, Torén K Rhine Study Group. Remission of asthma: a prospective longitudinal study from northern Europe (RHINE study). *Eur Respir J* 2007;30:62 65.
25 Jenkins M, Hopper J, Bowes G, Carlin J, Flander L, Giles G. Factors in childhood as predictors of asthma in adult life. *BMJ* 1994;309:90 93.
26 Hiroyuki M, Reiko M, Satomi H, Satoru T, Takahisa M, Hirokazu A. Relationship between bronchial hyperreactivity and asthma remission during adolescence. *Ann Allergy Asthma Immunol* 2009; 103:201 205.
27 Oswald H, Phelan P, Lanigan A, Hibbert M, Bowes G, Olinsky A. Outcome of childhood asthma in mid adult life. *BMJ* 1994;309: 95 96.
28 Vonk JPD, Boezen H, Grol M, Schouten J, Koeter G, Gerritsen J. Childhood factors associated with asthma remission after 30 year follow up. *Thorax* 2004;59:925 929.
29 Taylor D, Cowan J, Greene J, Willan A, Sears M. Asthma in remission: can relapse in early adulthood be predicted at 18 years of age? *Chest* 2005;127:845 850.
30 To T, Gershon A, Wang C, Dell S, Cicutto L. Persistence and remission in childhood asthma: a population based asthma birth cohort study. *Arch Pediatr Adolesc Med* 2007;161:1197 1204.
31 Upham J, James A. Remission of asthma: the next therapeutic frontier? *Pharmacol Ther* 2011;130:38 45.
32 Chen Y, Stewart P, Johansen H, McRae L, Taylor G. Sex difference in hospitalization due to asthma in relation to age. *J Clin Epidemiol* 2003;56:180 187.
33 Debley J, Redding G, Critchlow C. Impact of adolescence and gender on asthma hospitalization: a population based birth cohort study. *Pediatr Pulmonol* 2004;38:443 450.
34 Harju T, Keistinen T, Tuuponen T, Kivela S. Hospital admissions of asthmatics by age and sex. *Allergy* 1996;51:693 696.
35 AlMarri M. Asthma hospitalizations in the state of Qatar: an epidemiologic overview. *Ann Allergy Asthma Immunol* 2006;96: 311 315.
36 Prescott E, Lange P, Vestbo J. Effect of gender on hospital admissions for asthma and prevalence of self reported asthma: a prospective study based on a sample of the general population. Copenhagen City Heart Study Group. *Thorax* 1997;52:287 289.
37 Schatz M, Camargo C. The relationship of sex to asthma prevalence, health care utilization, and medications in a large managed care organization. *Ann Allergy Asthma Immunol* 2003;91:553 558.
38 Skobeloff E, Spivey W, St Clair S, Schoffstall J. The influence of age and sex on asthma admissions. *JAMA* 1992;268:3437 3440.
39 Mitchell E, Bland J, Thompson J. Risk factors for readmission to hospital for asthma in childhood. *Thorax* 1994;49:33 36.
40 Lee J, Haselkorn T, Chipps B, Miller D, Wenzel S; Tenor Study Group. Gender differences in IgE mediated allergic asthma in the epidemiology and natural history of asthma: Outcomes and Treatment Regimens (TENOR) study. *J Asthma* 2006;43:179 184.
41 The Childhood Asthma Management Program (CAMP): design, rationale, and methods. Childhood Asthma Management Program Research Group. *Control Clin Trials* 1999;20:91 120.
42 Titterington D, Smith A, Markov U. Statistical analysis of finite mixture distributions. New York: John Wiley & Sons; 1985.
43 Zannolli R, Morgese G. Does puberty interfere with asthma? *Med Hypotheses* 1997;48:27 32.
44 Balfour Lynn L. Childhood asthma and puberty. *Arch Dis Child* 1985; 60:231 235.
45 Nicolai T, Illi S, Tenborg J, Kiess W, v Mutius E. Puberty and prognosis of asthma and bronchial hyper reactivity. *Pediatr Allergy Immunol* 2001;12:142 148.
46 Vink N, Postma D, Schouten J, Rosmalen J, Boezen H. Gender differences in asthma development and remission during transition through puberty: the TRacking Adolescents' Individual Lives Survey (TRAILS) study. *J Allergy Clin Immunol* 2010;126:498 504.
47 Dey A, Bloom B. Summary health statistics for US children: National Health Interview Survey, 2003. *Vital Health Stat 10* 2005;Mar:1 78.
48 Balzano G, Fuschillo S, Melillo G, Bonini S. Asthma and sex hormones. *Allergy* 2001;56:13 20.
49 Canguven O, Albayrak S. Do low testosterone levels contribute to the pathogenesis of asthma? *Med Hypotheses* 2011;76:585 588.
50 Lamason RZP, Rawat R, Davis A, Hall JC, Chae JJ, Agarwal R, Cohen P, Rosen A, Hoffman EP, Nagaraju K. Sexual dimorphism in immune response genes as a function of puberty. *BMC Immunol* 2006;7: 1 14.